



## **Meteorology Research and Development**

### **The Assimilation of GPS Radio Occultation data into the Met Office global model**



**Technical Report No. 510**

**Michael Rennie**

*email: [nwp\\_publications@metoffice.gov.uk](mailto:nwp_publications@metoffice.gov.uk)*

**©Crown Copyright**



## Revision History

Date of this revision:

Date of next revision:

Revision Date	Previous Revision Date	Summary of Changes	Changes Marked
Dec 2007		First attempt	
Dec 2007		Revised after D Offiler review	
Jan 2008		Revised after R Saunders review	
Feb 2008		Small revision after S Healy review	

## Approvals

This document requires the following approval.

Name	Signature	Title	Date of Issue	Version

## Circulation

This document should be circulated to the following.

Name	Title	Date of Issue	Version

## **Abstract**

In the past few years GPS RO data has been made available to the Met Office with the quality and timeliness suitable for operational NWP. Since July 2006 we have been provided with data from the FORMOSAT-3/COSMIC constellation of six satellites, which substantially increased the amount of data available for operational assimilation. In this paper we will describe the current method for assimilating GPS RO at the Met Office, results from monitoring the data and results from forecast impact experiments. The forecast impact experiments cover two month-long periods in different seasons. The experiments evaluated the impact of the FORMOSAT-3/COSMIC data, assessed refinements to the observation plus forward model errors and experimented with altering the height range over which the data are assimilated. The resulting forecasts were verified against in situ observations and their own analyses. FORMOSAT-3/COSMIC GPS RO data was shown to give an appreciable positive impact which has led to the data being used operationally at the Met Office.

## 1. Introduction

GPS RO (Global Positioning System Radio Occultation) is a limb-geometry active remote sensing technique that provides accurate, all-weather, high vertical resolution profiles of measurements closely related to atmospheric variables; see Kursinski et al (1997, 2000) for a detailed description. The occultations from a constellation of, for example, six well-spread LEO satellites are provided with a pseudo-random spatial coverage over the Earth during a six hour assimilation window and the data is provided to regions where, for example, radiosondes (which are valued for providing accurate high vertical resolution information) are absent.

The radio occultation technique is based on determining the total refraction angle of a radio signal propagating through an atmosphere due to refractive index gradients along the path; see Melbourne et al (1994). The phase signal detected at the LEO is converted to an excess Doppler shift. The Doppler shift of the radiation is dependent on the dot product of the emitter (receiver) velocity vector with the emitted (received) ray path vector. A so called excess Doppler shift is introduced due to the ray following a different path between emitter and receiver in the presence of an atmosphere compared to the straight line path that is taken in a vacuum. One can relate the excess Doppler shift to the geometry of the ray path given precise information of the satellites' locations and velocities and with the assumption that the atmosphere's refractivity field is spherically symmetric. The bending angle can then be solved for iteratively; this is the geometric optics approach. Errors in the bending angles and corresponding impact parameters due to the spherical symmetry assumption are discussed in depth by Healy (2001). Radio holographic techniques that use the raw complex signal for deriving the Doppler shift are used in conditions of multi-path propagation, common in the moist troposphere, where the geometric optics approach is not applicable; see Kuo (2004).

The time measurements fundamental to the technique are calibrated very precisely by ultra stable atomic clocks and thus no additional satellite or inter-satellite calibration is required. Consequently the observations have high accuracy (i.e. degree of veracity) and high precision (i.e. degree of reproducibility), Schreiner et al (2007). GPS RO is considered accurate enough to assimilate without bias corrections and thus has great potential for decreasing model biases in the upper troposphere and stratosphere. Like radiosondes, GPS RO should therefore improve the assimilation of other remotely sensed data that require bias correction to the NWP model.

Forecast impact experiments have shown that GPS RO can provide positive impact on global NWP models with relatively few occultations, especially in the upper troposphere and lower stratosphere, see Healy (2005a, 2005b and 2006). This report will build on these reports and will describe the assimilation of GPS RO at the Met Office with a view towards the operational assimilation of the data. We will show the results of forecast impact experiments using data from the recently launched radio occultation mission: the FORMOSAT-3/COSMIC constellation, also CHAMP and GRACE-A data was used in some of the trials. We will refer to the FORMOSAT-3/COSMIC constellation as simply COSMIC from now on.

The processed GPS RO observations provided to operational NWP centres for assimilation are the bending angle of the ray as a function of impact parameter and the refractivity of the atmosphere as a function of geometric height (refractivity is derived from bending angle as a function of impact parameter). Both vertical coordinates are with reference to the WGS-84 ellipsoid. Either approach will provide meteorological information via direct data assimilation;

refractivity can be forward modelled from temperature, total pressure and water vapour pressure and subsequently bending angles can be forward modelled from fields of refractivity.

Both methods have their advantages and disadvantages, although it is generally believed that bending angle is the best quantity to assimilate, see Eyre (1994). Currently at the Met Office we only have the capability for the operational assimilation of refractivity (using a 1D observation operator); a future improvement will be to enable 1D bending angle assimilation. At the time of writing several NWP centres are using 1D bending angle operators (including ECMWF and Meteo France), NCEP use a 1D refractivity operator (although they have the option to use 1D bending angle, Cucurull (2006)).

Over the past few years GPS RO data has become available in sufficient quantity, timeliness and quality to be used in operational NWP. CHAMP data provided by GFZ became available in near real-time on 22<sup>nd</sup> February 2006 and GRACE-A on the 28<sup>th</sup> May 2006. After showing positive results in forecast impact experiments (see Buontempo et al (2007) submitted) and satisfactory integration into a parallel suite (PS12), CHAMP and GRACE-A data processed by GFZ were made operational on the 26<sup>th</sup> September 2006. As far as we are aware the Met Office was the first NWP centre to assimilate GPS RO operationally. Unfortunately the GFZ data later (17<sup>th</sup> November 2006) had to be withdrawn from operations due to quality issues with the GFZ processing at that time. The OPS (Observations Processing System) failed to black-list the “bad” data, but was later modified to use a stricter quality control scheme. Since COSMIC has made available significantly greater volumes of data, the use of CHAMP and GRACE-A has become less of a priority, although if the quality and data flow is seen to be adequate then there is no reason not to assimilate the data.

MetOp-A was launched on the 19<sup>th</sup> October 2006, carrying the GRAS RO instrument. Although the raw GRAS data is reported to be of high quality, the operational ground processing is not yet (at the time of writing) producing bending angle profiles of adequate scientific quality. A major future aim is to assimilate GRAS data when the data is processed to a satisfactory quality. The GRAS instrument has a better SNR than other currently available GPS RO receivers due to larger antennas and the data has the potential to be used to higher altitudes.

The UCAR-processed data from the COSMIC constellation of six satellites became available on 28<sup>th</sup> July 2006 and given the great volume of data we were eager to begin trialling it for operational use. Trials of COSMIC for August 2006 showed mixed results; this may have been due to the satellites being poorly spread at the time, the observation errors were not optimised and there may also have been bugs in the early processing and consequently this delayed the operational use of COSMIC. Trials using a November/December 2006 control showed a positive impact (as documented in this report); hence the data began to be used operationally at the next available opportunity which was 15<sup>th</sup> May 2007 (following PS15). Unfortunately COSMIC was withdrawn from operations due to model crashes on 11<sup>th</sup> June 2007, however these crashes were later shown to be unrelated to GPS RO and COSMIC was reinstated with PS16 which went operational on 14<sup>th</sup> August 2007.

As with all meteorological data used in operational NWP, the timeliness is critical. Currently (Jan 2008) around 80-90 % of the COSMIC data arrives in the MetDB within 3 hours and the statistics for GFZ processed CHAMP and GRACE-A are even better (> 95 % within 3 hours). We operationally use only roughly 50% of the COSMIC occultations in the main global runs due to the constraints of a model cut-off time; a much greater proportion are used in the update global runs which are used to produce the background (first guess) for the next main global run.

We initially assimilated only four of the six COSMIC satellites; the use of all available COSMIC became operational following PS17 (27<sup>th</sup> November 2007). Four were chosen as a cautious response to the satellites then being in similar orbits and later a global model problem (June 2007 crash as mentioned) led to concerns over using too much data over Antarctica which postponed an earlier increase to assimilate all six.

The aim of this paper is to explain how GPS RO is used at the Met Office, to present some results from monitoring of the data and to describe the assimilation experiments that were ran to assess the impact GPS RO has on NWP with the intention of using it operationally. It is structured as follows. Section 2 describes how the observations are assimilated at the Met Office. Section 3 presents some results from monitoring the data. Section 4 discusses the details of the forecast impact experiments. Results of the impact of GPS RO data on the global NWP model are discussed in Section 5. The discussion and conclusions are presented in Sections 6 and 7.

## 2. Technical Details for GPS RO Assimilation

### a. *The Met Office System*

At the Met Office there are two main steps to assimilating data that concern this paper. They are implemented by two computer systems; the Observations Processing System (OPS) followed by the Variational Data Assimilation System (VAR). The OPS acquires the observation data from the MetDB (database of received observations) after which any pre-processing of the data and quality control checks can be performed. The data is then passed to VAR to be assimilated (currently using 4D-Var) within which the output of the OPS quality control is used to avoid assimilating data which is believed to contain gross errors.

The GPS RO quality control in the OPS uses a 1D-Var procedure. Variables such as initial and final cost function, the number of iterations, and the difference of solution from background are calculated and if the values lie outside what is seen as acceptable we black-list the data to avoid it being used in VAR. The 1D-Var is also useful per se for monitoring the variational assimilation of GPS RO data e.g. observing the effects on the pressure and specific humidity state vector and hence the derived temperature. Monitoring plots based on the output of the 1D-Var and observation minus background statistics are produced in near real-time every six hours and are used for checking data quality. Some of these plots are made publicly available on the GRAS SAF monitoring website (<http://monitoring.grassaf.org>).

### b. *The data*

Currently, the bending angle and refractivity data from UCAR are provided on 300 vertical levels from ~60 km down to where the occultation is lost in a setting occultation (or starts in a rising occultation). GFZ provide their data on 247 fixed levels as determined by the ROPP thinner software that they use, data absent from a particular level is set as missing. Ideally UCAR would also provide their data on a fixed set of levels that reflects the information content of the measurement. If a UCAR processed occultation is cut short (which does happen occasionally) then we still receive 300 levels, which then will have an unnecessarily high vertical sampling. It is important to stress that this creates no problems with our assimilation system as we take into account vertical correlations in our  $\mathbf{R}$  matrix for refractivity; it just leads to extra computations and when monitoring we must interpolate onto our own fixed set of height levels. GRAS profiles will be provided on the same 247 fixed levels used by GFZ.

Bending angle is processed less than refractivity which is an advantage in some respects. The transform from bending angles to refractivity is via the Abel transform. This integrates bending angle times a weighting factor as a function of asymptotic miss distance with an upper integration limit of infinity. At high impact parameters observed bending angle becomes too noisy to be used directly in the Abel integral since it would propagate these high altitude bending angle errors to lower altitude refractivity errors. To mitigate this, a priori information is used to smooth the noisy bending angles e.g. climatology or model forecasts can be used. The influence of a priori can be significant in the refractivity data kilometres below where it was used and since we do not want to assimilate a priori then care must be taken when choosing an upper cut-off height. The depth of its influence is unique to the processing of each occultation,

e.g. it will depend on the initial noise of the bending angles and what technique is used to “blend” the a priori with the observation.

Bending angle assimilation (using bending angles prior to smoothing with a priori) in an altitude range below the noise (e.g. below ~40 km, the current ECMWF upper cut-off) avoids the assimilation of a priori as in refractivity. However the Met Office global model biases at the altitudes where a priori is influencing refractivity are seen to be greater than processing biases seen between UCAR and GFZ, therefore it is perhaps justified to use refractivity at these altitudes (see Section 3).

Another disadvantage to refractivity profiles is that the correlations in the observation errors are much larger than bending angle due to the averaging effect of the Abel Transform integral. Therefore we take into account these refractivity correlations in the covariance matrix whereas bending angle error correlations are probably small enough to be neglected. The main disadvantage to bending angle is that the forward operator is more complicated and more computationally expensive, although it is still relatively small in comparison with other satellite data types e.g. ATOVS radiance assimilation.

### *c. Observation Operators*

Currently, at the Met Office the assimilated observation is refractivity as a function of geopotential height. The observation operator is used in the OPS 1D-Var and in the GPS RO part of the 4D-Var code (VAR) but with subtle differences; that is VAR uses pressure and relative humidity as the state vector whereas OPS uses pressure and specific humidity. In VAR it may now be possible to use specific humidity in the state vector thus avoiding an iterative calculation of the layer mean temperature from the layer mean virtual temperature. The VAR code is simpler than the OPS as only the GPS RO observation penalty and its gradient with respect to the state vector are calculated while a complete minimisation procedure is required in the OPS 1D-Var.

The data providers (e.g. UCAR, GFZ, DMI) supply each occultation as a vertical profile of refractivity with corresponding geometric heights above the WGS-84 ellipsoid at a given latitude and longitude. The geometric heights are converted to geopotential heights using a routine in the OPS; the method used is written for the WGS-84 ellipsoid (see <http://mtp.jpl.nasa.gov/notes/altitude/altitude.html>). The data is then in a format suitable for use in the forward model.

We use a local 1D refractivity operator: the model equivalent observations are calculated by interpolating model fields of pressure and specific (relative in VAR) humidity given on model geopotential height levels to the observation location i.e. the latitude and longitude supplied with the occultation, from which a local profile of refractivity can be calculated. 2D effects in the occultation plane (to take into account the limb configuration of the measurement) are not accounted for. This forward model results in errors when strong horizontal gradients of refractivity are present along the ray path e.g. weather fronts and other spherically asymmetric features in the troposphere. However, such events are relatively rare. To take into account these horizontal gradients in a 2D forward model we require a background that already contains information on the horizontal gradients to sufficient accuracy; however the global model horizontal resolution may limit just how well represented they are.



The use of a 2D bending angle operator at ECMWF was found only to be important in the meteorological scenarios with strong horizontal gradients (see Healy et al (2007)) but in these scenarios the 1D operator error can be as much as ~20% in bending angle. The 2D method is also computationally more expensive and much greater quantities of background data are required. The infrastructure to use 2D operator at the Met Office is not yet in place. Hence using a 1D operator with sufficiently large observation plus forward model errors ( $R$  matrix) low down is the preferred method at present.

A next step for potentially improving the assimilation may be to use a local 1D bending angle observation operator instead of refractivity for the reasons given previously. Of course this method still suffers from not taking into account horizontal gradients. Code for a local 1D bending angle operator is already available from ROPP and a ROPP 2D bending angle operator is in the process of being written.

#### *d. Met Office refractivity operator*

The following section describes the 1D refractivity observation operator after the global model background data has been interpolated to a vertical column at the observation location (tangent point). The Met Office unified model provides information on a staggered height grid (Figure 1).

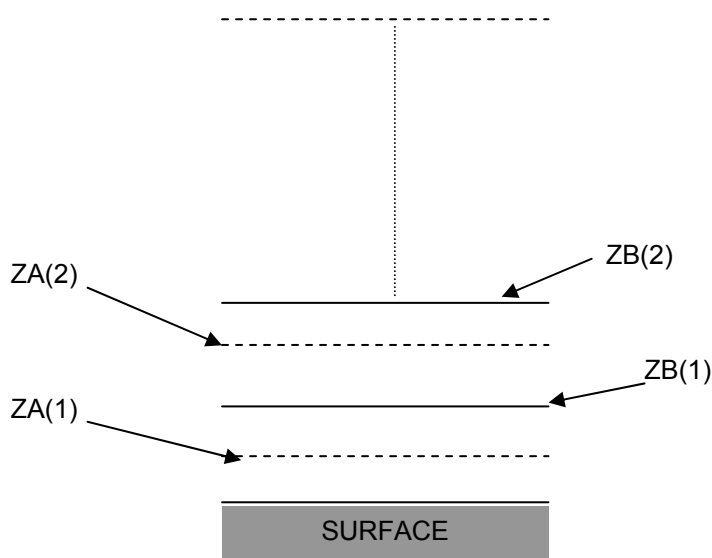


**Figure 1.** The new dynamics staggered height grid.

It gives pressure and density information on “rho” or “A” levels and potential temperature and humidity information on the “theta” or “B” levels. The state vector in OPS is pressure on “A” levels and specific humidity on “B” levels whilst in VAR it is pressure on “A” levels and relative humidity on “B” levels (note this may be changed to specific humidity in the future). The first “B” level is situated between the first and second “A” levels, at a height ZB(1). Similarly the second

“B” level is between the second and third “A” levels and so on. Refractivity is calculated on the “B” levels and then interpolated to the arbitrary observation heights provided. The method below is deemed to be the most consistent with the dynamics of the model.

- The Exner pressure on the “A” levels are calculated using the standard definition,

$$\Pi A(i) = \left( \frac{PA(i)}{P_0} \right)^\kappa \quad (0.1)$$

where,

$$\kappa = \frac{R}{c_p} \quad (0.2)$$

and  $P_0$  is reference surface pressure (set at  $1 \times 10^5$  Pa).  $R$  ( $287.05 \text{ J kg}^{-1} \text{ K}^{-1}$ ) is the specific gas constant for dry air and  $c_p$  ( $1005 \text{ J kg}^{-1} \text{ K}^{-1}$ ) is the specific heat capacity of dry air at constant pressure.

- The Exner value on the  $i^{\text{th}}$  “B” level is calculated assuming linear variation with geopotential height,

$$\Pi B(i) = \alpha \Pi A(i) + (1 - \alpha) \Pi A(i + 1) \quad (0.3)$$

where

$$\alpha = \frac{ZA(i + 1) - ZB(i)}{ZA(i + 1) - ZA(i)} \quad (0.4)$$

- The pressure on the  $i^{\text{th}}$  “B” level is then,

$$PB(i) = P_0 (\Pi B(i))^{1/\kappa} \quad (0.5)$$

- The layer mean virtual temperature is found by solving the hydrostatic equation when the potential temperature is constant across the layer,

$$TB_v(i) = \frac{g \Pi B(i)}{c_p} \left( \frac{ZA(i + 1) - ZA(i)}{\Pi A(i) - \Pi A(i + 1)} \right) \quad (0.6)$$

where  $g$  ( $9.80665 \text{ ms}^{-2}$ ) is the mean acceleration due to gravity at the earth’s surface.

- The layer mean temperature is then,

$$TB(i) = TB_v(i) / (1 + (\frac{1}{\varepsilon} - 1)QB(i)) \quad (0.7)$$

where  $\varepsilon$  is the ratio of the molecular mass of water vapour and dry air, and  $QB(i)$  is the specific humidity of the  $i^{th}$  "B" level.

- In VAR the calculation of layer mean temperature (equation (0.7)) is complicated by the state vector being relative humidity (RH) on the "B" levels and not specific humidity (q). As the conversion from RH to q involves calculating the saturation vapour pressure ( $e_s$ ) which itself is a function of temperature, then the layer mean temperature must be solved for iteratively. This is done using the Newton-Raphson method. The equation for q is:

$$QB(i) = \frac{\varepsilon RH(i) e_s(i)}{PB(i)} \quad (0.8)$$

$e_s$  and its gradient with respect to temperature are calculated from a lookup table given TB.

- By rearranging equation (0.7) we define a function  $f$  for which we want to find the root (i.e. find TB such that  $f(TB)=0$ ):

$$f(TB(i)) = TB(i) - TB_v(i) / (1 + (\frac{1}{\varepsilon} - 1)QB(i)) \quad (0.9)$$

- Starting with a first guess of

$$TB_1(i) = TB_v(i) \quad (0.10)$$

we solve for TB iteratively using

$$TB_{n+1}(i) = TB_n - \frac{f(TB_n)}{f'(TB_n)} \quad (0.11)$$

The iteration loop stops after five iterations or if the change in the solution is less than 0.1 K.

- The refractivity on  $ZB(i)$  is then

$$NB(i) = \frac{aPB(i)}{TB(i)} + \frac{bPB(i)QB(i)}{TB(i)^2(\varepsilon + (1 - \varepsilon)QB(i))} \quad (0.12)$$

where

$$\begin{aligned} a &= 77.6K / hPa \\ b &= 3.73 \times 10^5 K^2 / hPa \end{aligned} \quad (0.13)$$

- The  $j^{th}$  refractivity at the observation height  $ZOBS(j)$  between the  $i^{th}$  and  $(i+1)^{th}$  "B" levels is calculated assuming that refractivity varies exponentially with height,

$$N(j) = \exp(\beta \text{LOG}(NB(i)) + (1 - \beta) \text{LOG}(NB(i + 1))) \quad (0.14)$$

where

$$\beta = \frac{ZB(i + 1) - ZOBS(j)}{ZB(i + 1) - ZB(i)} \quad (0.15)$$

The full non-linear forward model as described above is approximated by its tangent linear model on some of the iterations within VAR to make the minimisation problem quadratic (the non-linear model is run every tenth iteration).

### 3. Monitoring Results

Considerable effort has been put into monitoring GPS RO data in preparation for its use operationally. The monitoring is mostly based on observation minus background statistics (O-B), where O is the observation and B is the forward modelled observation equivalent derived from a global model 6 hour forecast. In this section some of the interesting features of the O-B statistics are discussed.

#### a. General behaviour

Figure 2 shows a typical plot of refractivity (O-B)/B statistics using one month's global data.

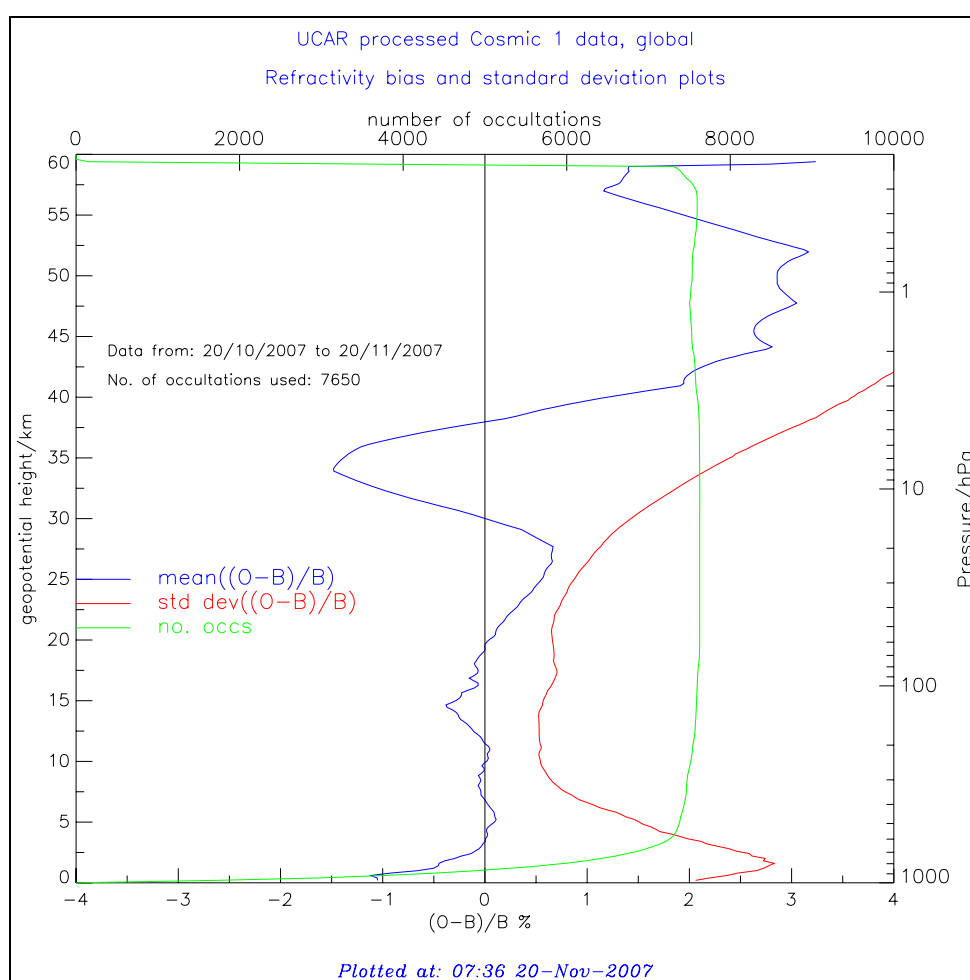


**Figure 2.** Mean and standard deviation of refractivity (O-B)/B and the number of occultations used at each height level for one month's global data for FM1.

Notice the negative bias and large standard deviation at the bottom of the profile (< 3 km geopotential height). This bias in refractivity (and also bending angle) data is known to be

associated with the observation processing in conditions of sharp vertical gradients in refractivity that can lead to super-refraction, see Ao et al (2003). Forward modelling errors i.e. a failure of the 1D observation operator to represent the observation correctly, become increasingly important in the lower troposphere. As discussed previously, the observation operator derives refractivity from a vertical profile of model fields at the tangent point, i.e. a local operator. Therefore the variation of temperature and humidity fields in the horizontal (both along and perpendicular to the path of the ray) in the lower troposphere over the horizontal range of a GPS radio occultation measurement fails to be taken into account; this leads to the high (O-B)/B standard deviation.

The negative bias at ~15 km is believed to be associated with model bias at the tropopause (mainly in the tropics). The 'S' shape bias from ~20 – 40 km is a model bias also, as will be shown later in this section. The large biases above 40 km are where the refractivity increasingly consists of a priori climatology used in smoothing the bending angles.

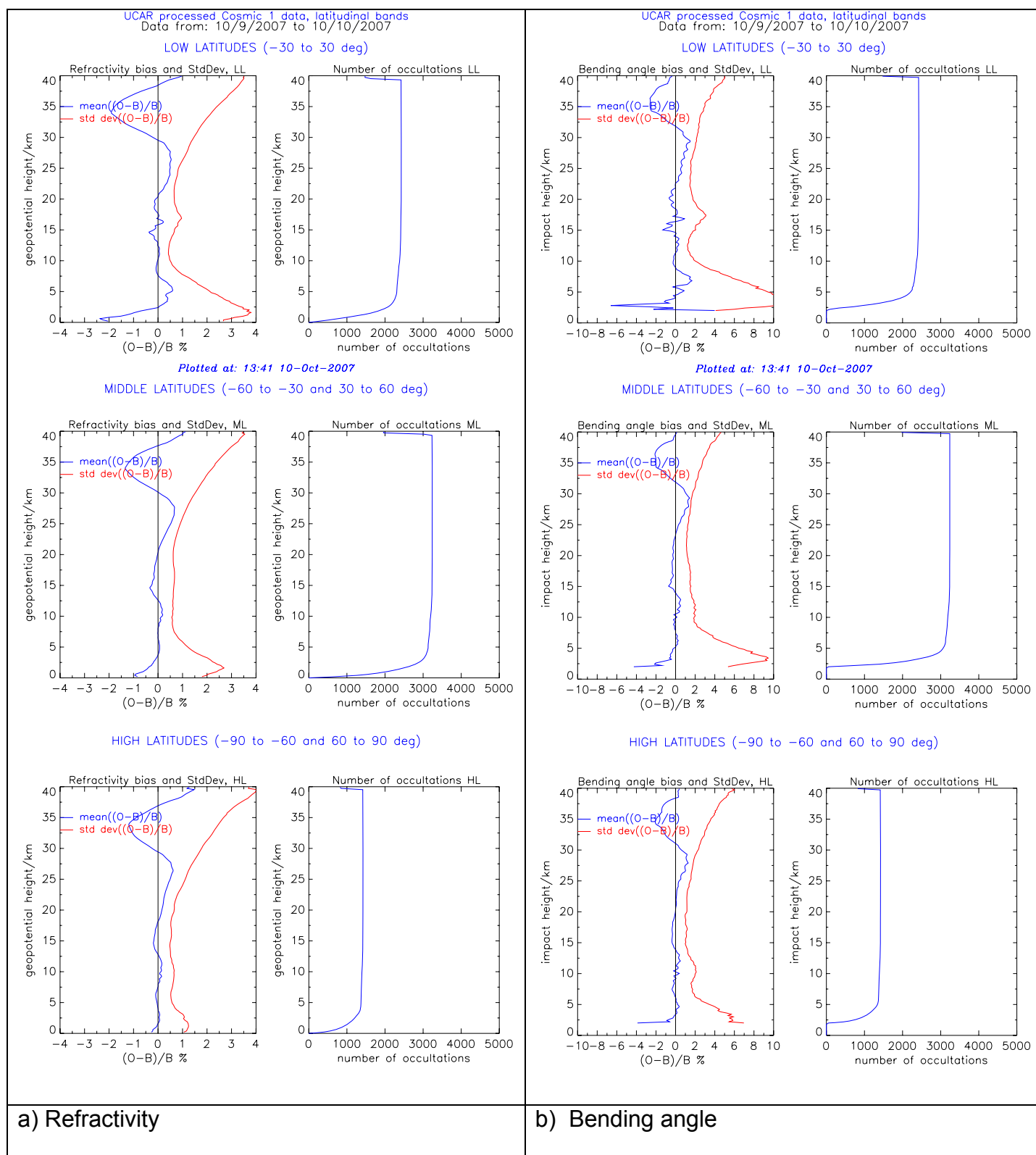


**Figure 3.** Plot a) is the same data as in figure 2 but separated into latitude bands. Plot b) shows the equivalent of a) using bending angles for the same occultations (note the larger scale).

If we split the data of Figure 2 into latitude bands (low latitudes  $|\text{lat}| \leq 30$  degrees, middle latitudes  $30 < |\text{lat}| \leq 60$  and high latitudes  $|\text{lat}| > 60$  degrees) as in Figure 3a, then we can see that the standard deviation in the lower troposphere is largest at low latitudes due to the higher water vapour in the atmosphere. Notice also that the negative bias in refractivity is much larger at low latitudes due to sharp refractivity gradients being most prevalent here; see Figure 4, which shows that large vertical gradients of refractivity are most common over sea in bands either side the equator. Notice in Figure 3a that the bias at ~15 km is sharper at low latitudes but there is still some evidence for it at middle latitudes. The high altitude 'S' shape bias is present in all bands.

If we look at Figure 3b which is equivalent to Figure 3a but for bending angle instead of refractivity we see similar features except the magnitude of standard deviations and biases are larger for bending angle (note different scale), we expect this because of the smoothing the Abel integral introduces when transforming from bending angle to refractivity.

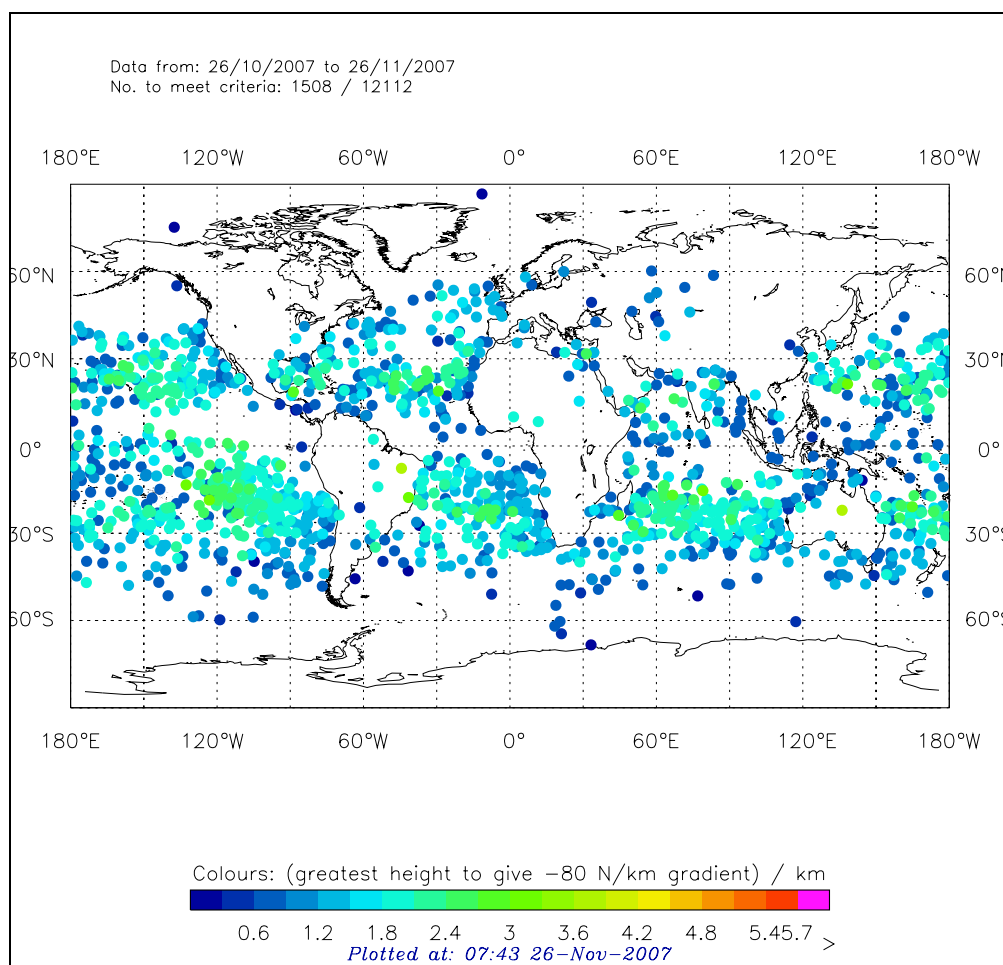


**Figure 4.** The distribution of model refractivity profiles (at FM4 locations during 1 month) that had vertical refractivity gradients  $< -80 \text{ N/km}$ . Also the highest geopotential height at which this threshold was reached is shown by colour bar.



*b. Met Office global model bias*

Notice from Figure 3b the 'S' shape bias is present in bending angle space as well as refractivity which backs the assumption that it is a global model bias rather than, for example, an error in processing to refractivity. This 'S' shape bias can be seen in a zonal plot of bending angle  $(O-B)/B$  as shown in Figure 5 (top image, see the negative band of bias at ~30 - 35 km). Another feature to notice is the negative bias at the lowest impact heights spreading over a broad range of latitudes but most intense in the tropics (note there is more negative bias in the northern hemisphere than in the southern hemisphere due to the season being the northern hemisphere summer and consequently the atmosphere has more water vapour there). Also notice a small positive bias at ~6 km at around 10 degrees north, this feature can be seen in the low latitude plots in Figure 3. It appears that this bias may be due to the model currently failing to resolve temperature inversions more commonly seen in convectively active regions of the tropics. This was noticed when comparing individual cases of GPS RO profile 1D-Var temperature results to nearest radiosonde temperature data which can resolve these features. The model backgrounds did not show the inversion yet the 1D-Var solutions did along with the radiosonde data (a more rigorous study of this should be performed). The patch of high standard deviation at ~15-20 km over the tropics is associated with the mismatch between RO and model in the tropical tropopause as mentioned previously (note this is not as distinct in the refractivity zonal plots, again due to the Abel integral smoothing bending angle features). The 'S' bias structure (between ~35 -40 km) can be seen to vary with the seasons and appears to have a larger magnitude over the winter pole. Recent test have shown that the 'S' shape bias is very sensitive to changes in the RTTOV forward model for radiance assimilation which indicates that radiance data is very dominant at these altitudes; this demonstrates that perhaps assimilating refractivity at these altitudes would be useful for tuning radiance bias correction.

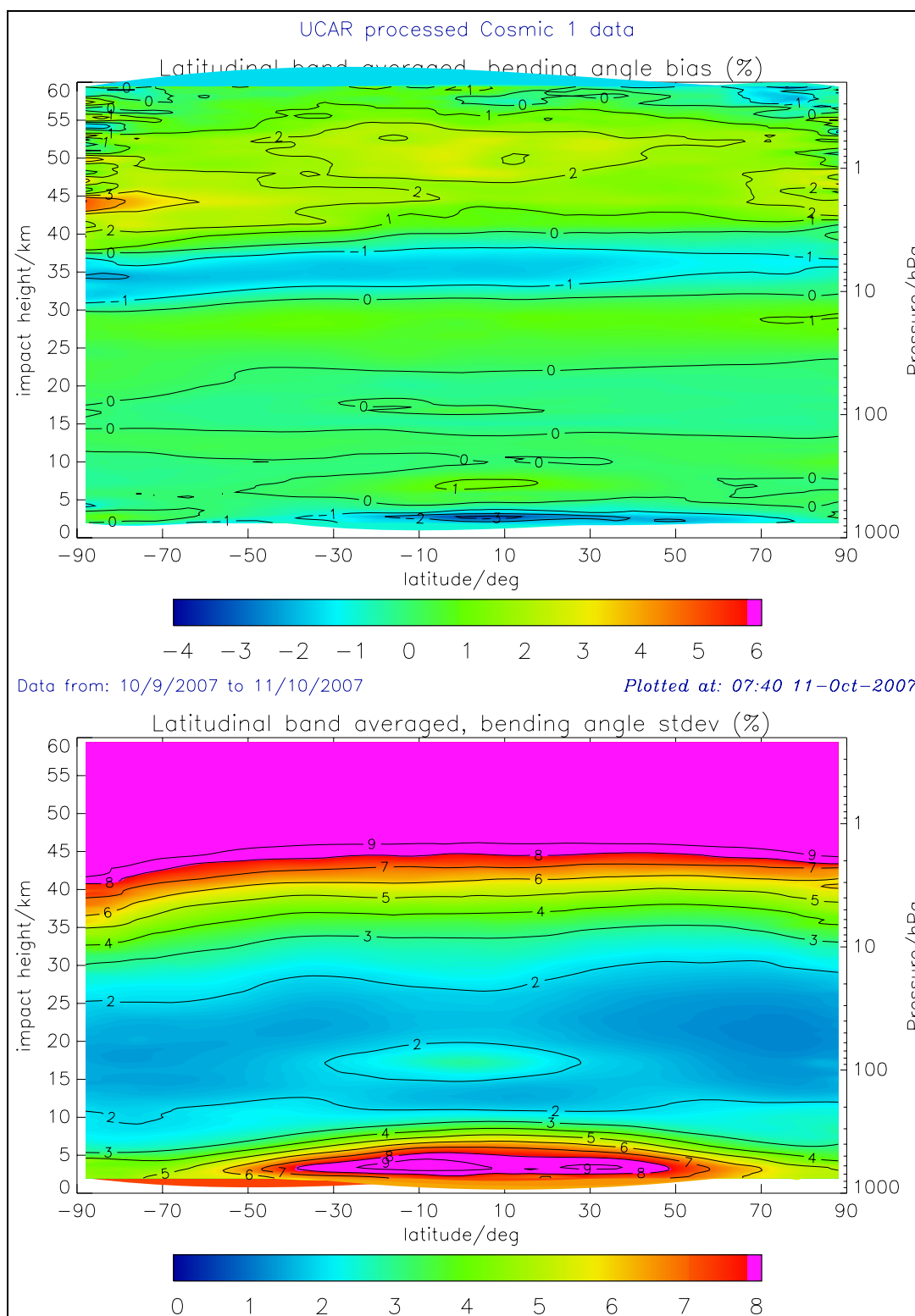


**Figure 5.** Zonal plot of bending angle (O-B)/B mean (top) and standard deviation (bottom) for FM1.

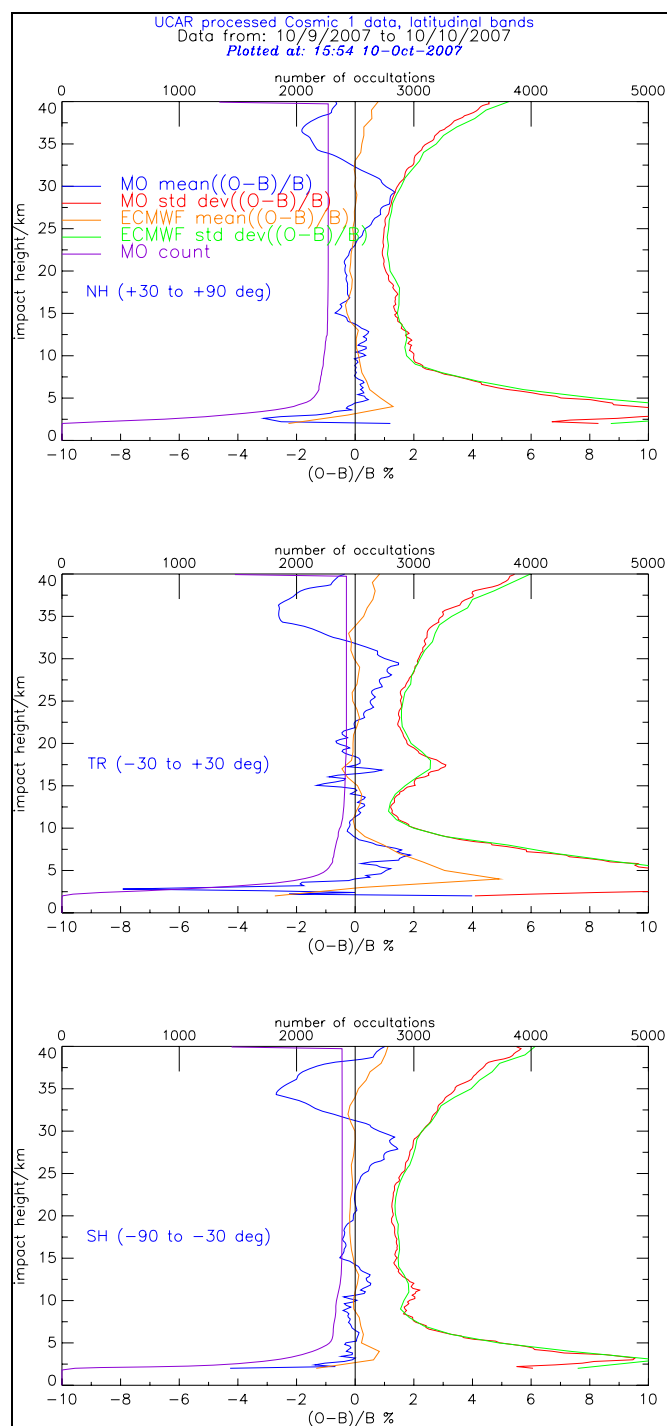


**Figure 6.** Bending angle (O-B)/B mean and standard deviation split into hemispheres and tropics using FM1. Met Office and ECMWF data are shown, see legend at the top.

Figure 6 is a comparison of the Met Office bending angle  $(O-B)/B$  to the equivalent from ECMWF (note the B is a 12 hour forecast for ECMWF). Figure 6 provides confirmation that the 'S' shape bias is unique to the Met Office global model as it cannot be seen in the ECMWF statistics. Generally the Met Office biases are worse than ECMWF's except in the lower tropopause. Also note how similar the standard deviation is for both. The Met Office plot uses different quality control criteria to the ECMWF plot and therefore the comparison will not be perfect, although the quality control is fairly relaxed for both ( $> 80\%$  difference rejected at MO,  $> 8 \times (\text{predicted error})$  difference rejected at ECMWF), we therefore believe it is still a fair comparison.

### c. Land/sea comparison

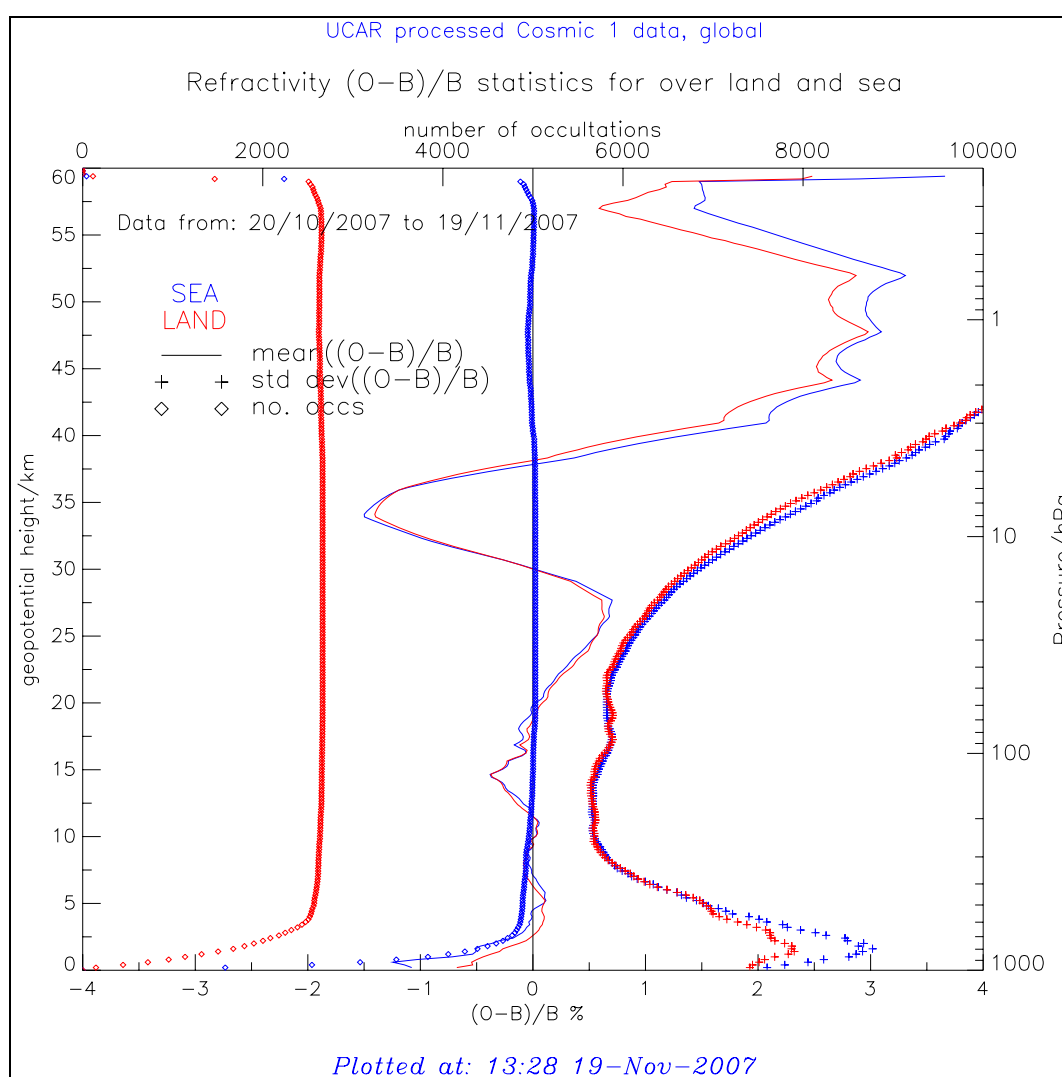


**Figure 7.** Plot of refractivity  $(O-B)/B$  split into occultations over land and over sea, made using a land/sea mask with a horizontal resolution of 1 by 1 degrees in latitude and longitude.

In Figure 7, below 40 km, one can see subtle differences in the bias and standard deviation over land compared to sea; this is most obvious in the bias and standard deviation at the bottom of the profile. This is probably due to differing boundary layer conditions over land and sea, with super-refraction conditions being more common over sea (Figure 4); this would therefore explain the larger negative bias seen over sea in Figure 7. This behaviour is replicated with other satellites. The high altitude differences are where the refractivity is dominated by climatology a priori and are therefore irrelevant.

#### *d. Processing differences*

Since we have CHAMP data processed by different sources (GFZ and UCAR) this provides an opportunity to see how different processing algorithms influence the observations, see also Engel (2005). Figure 8 shows the difference between UCAR and GFZ processed CHAMP data for refractivity (a) and bending angle (b) from 1278 matches. They are matched by searching for occultations within 1 degree in latitude and longitude and 72 minutes in time. The first thing to notice is that CHAMP UCAR and CHAMP GFZ are unbiased for a reasonable proportion of the profiles, in particular the bending angle which supports the suggestion of using bending angle for detecting climate change signals (see Ringer et al (2007)). Looking in detail one can see that similar patterns appear in both bending angle and refractivity but with differing magnitudes. Refractivity is smoother due to the Abel transform as expected.

The bias in refractivity at the top of the profile (~2% at 40 km) is larger than bending angle (~0.8%) and extends further down (to ~25 km compared to ~32 km for bending angle). Perhaps this refractivity bias is partly due to differing a priori climatology (GFZ use MSIS and UCAR use CIRA) propagating down or perhaps some influence from the Abel integral on the bias that exists already in bending angle space. We do not yet know which processing method is more accurate in the biased region. Perhaps of some concern are the small biases (relative to the standard deviation) seen between 0 and 10 km for refractivity and bending angle.

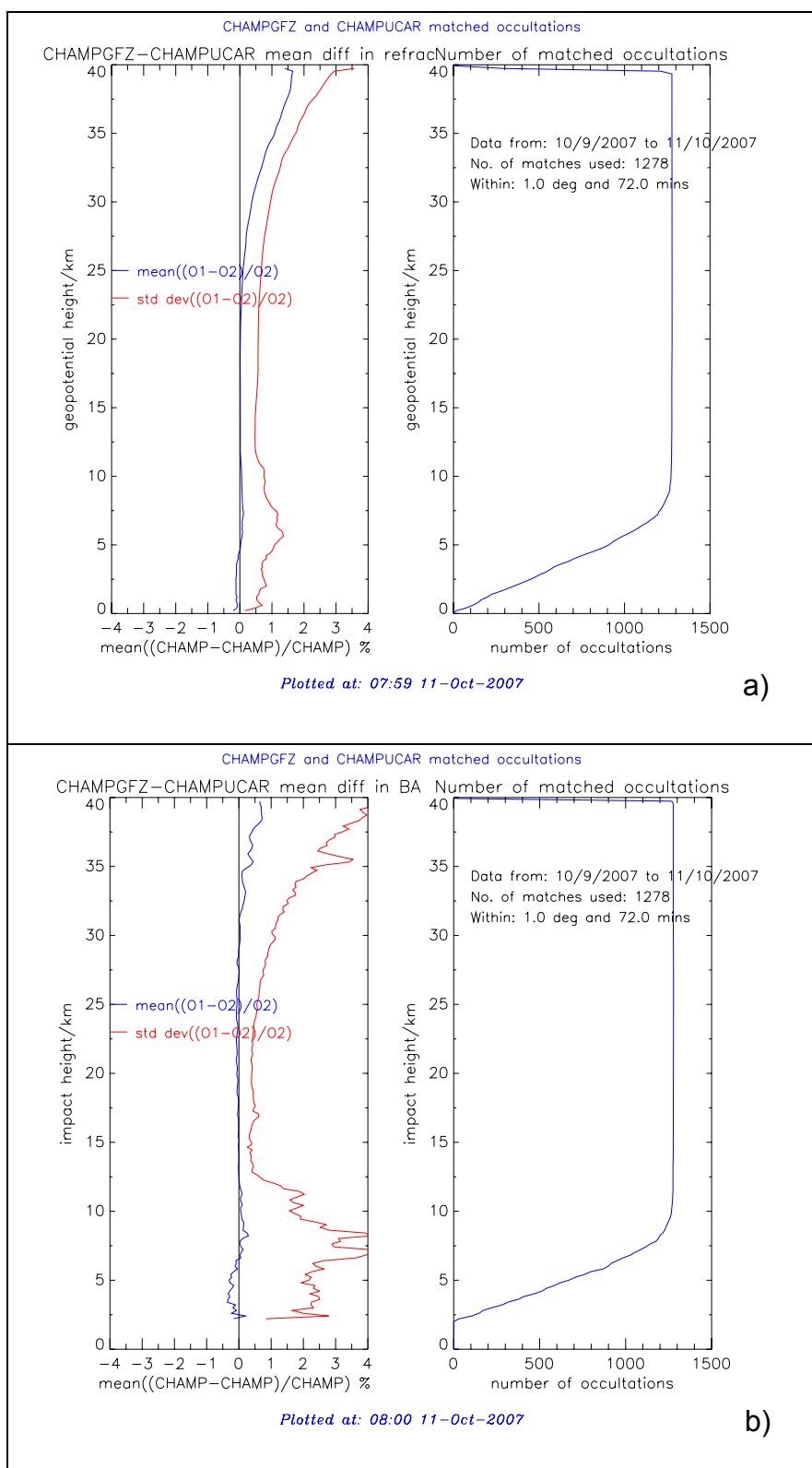


**Figure 8.** Matched UCAR and GFZ CHAMP data, a) is refractivity and b) is bending angle. The occultations were matched within 1 degree in latitude and longitude and 72 minutes in time.

A statistic that gives some information on how the observation errors are correlated is the vertical correlation of  $(O-B)/B$ . First the covariance  $\sigma_{ij}$  is calculated then the correlation coefficient  $r$  can be obtained:

$$x_i = \frac{(O_i - B_i)}{B_i} \quad (0.16)$$

$$\sigma_{ij} = \langle x_i x_j \rangle - \langle x_i \rangle \langle x_j \rangle \quad (0.17)$$

$$r = \frac{\sigma_{ij}}{\sigma_i \sigma_j} \quad (0.18)$$

Clearly this contains correlations of the global model via the forward model to observation space; however given we do not have truth it still provides some useful insight. Over monthly averages we can assume the background to be fairly similar for different satellites. However note that the CHAMP and GRACE-A satellites are constrained to sampling around small ranges of local solar times (not the same ranges for CHAMP and GRACE-A), which may have some influence on the B component, individual COSMIC satellites sample a broader range of local solar times over a month. We would assume differences between satellites/processing can be mostly attributed to the O component. The vertical correlation of FM1 refractivity  $(O-B)/B$  is shown in Figure 9a. One can see that the correlation scale length is fairly small up to ~20 km but higher than this we see much larger scale lengths which may be due to the combination of a priori climatology and the Abel integral. One may assume that the 'S' shape bias would cause these high correlations but a comparison to the correlations of FM1 bending angle which also has the 'S' shape bias for the same period shows much smaller correlations, see Figure 9b.

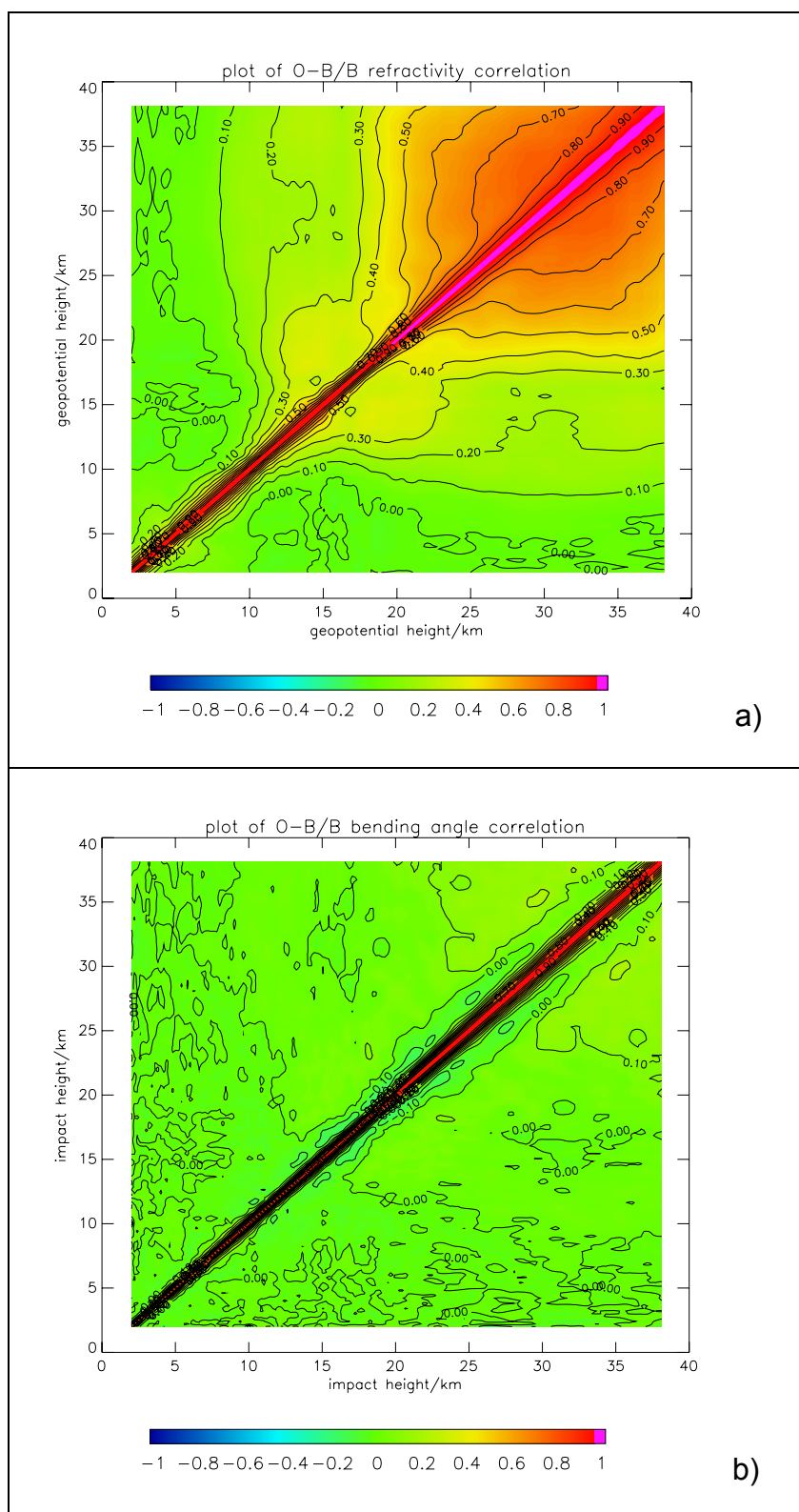


**Figure 9** The vertical correlation in refractivity (O-B)/B (a) and bending angle (b). This is using UCAR processed FM1 data for the period 11 September till 11 October 2007.



In fact the upper correlations of refractivity vary noticeably between COSMIC satellites and with time unlike the bending angle correlations. We suggest this is down to varying SNR of the satellites and thus how much quality control is performed and a priori is used by UCAR. For example FM6 had a period of much smaller upper correlations than the other COSMIC satellites but it was known to be having technical problems at this time, perhaps suggesting FM6 was receiving stricter quality control. Another point to note is that the refractivity correlations of CHAMP and GRACE-A processed by GFZ appear very similar whereas CHAMP processed by UCAR appears somewhat different, see Figure 10 and Figure 11. GFZ processed refractivity has larger correlations around 15-20km than UCAR; the differences in processing that lead to these differing correlations should be investigated. Bending angle looks very similar for all satellites/processing. These correlation plots demonstrate that there may be some issues to resolve regarding the processing of bending angles to refractivity in a consistent manner.

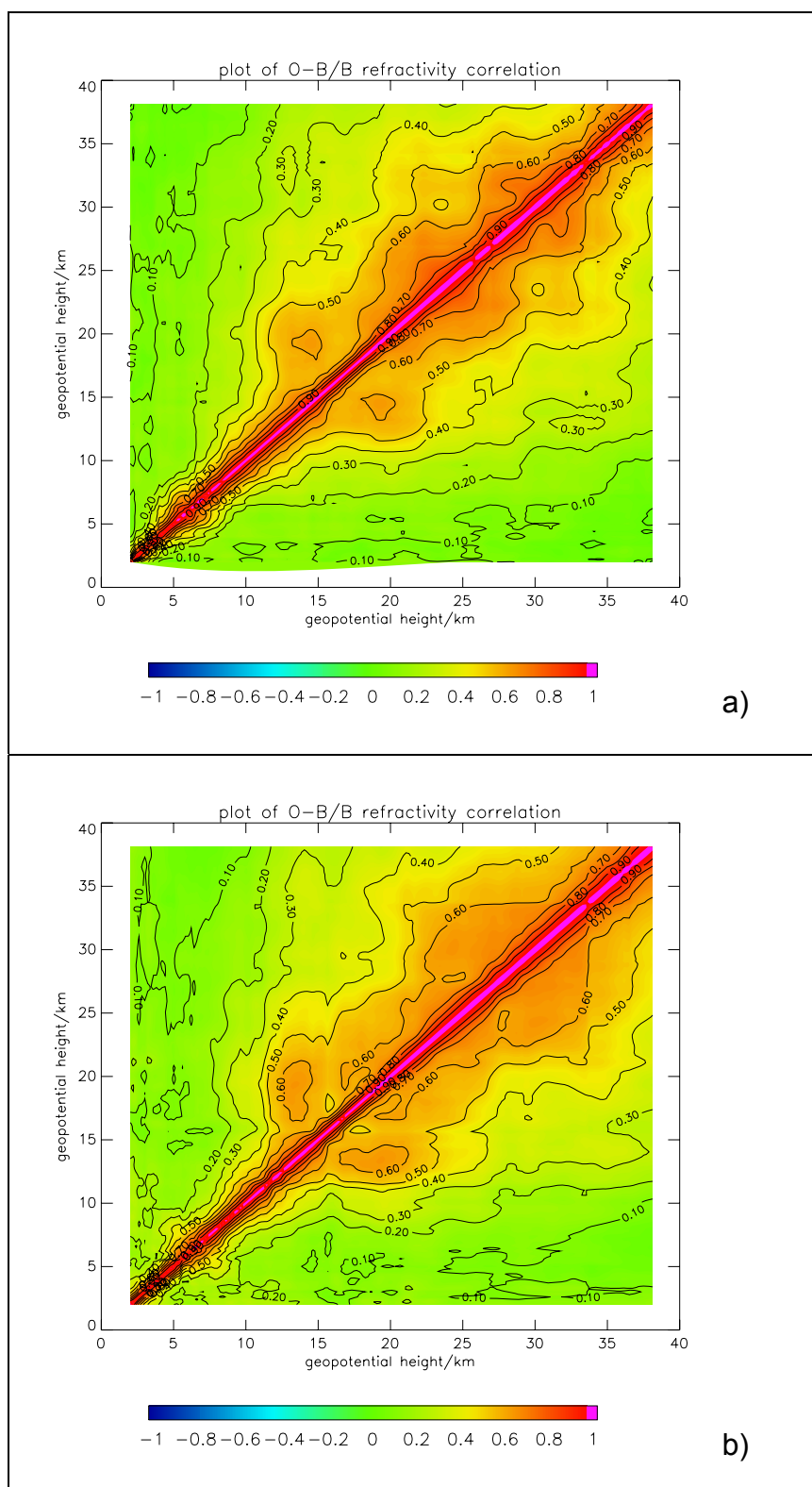


**Figure 10.** Plot of the vertical correlation in refractivity  $(O-B)/B$ . This is using GFZ processed CHAMP data (a) and GFZ GRACE-A data (b) for the period 9 September till 9 October 2007.

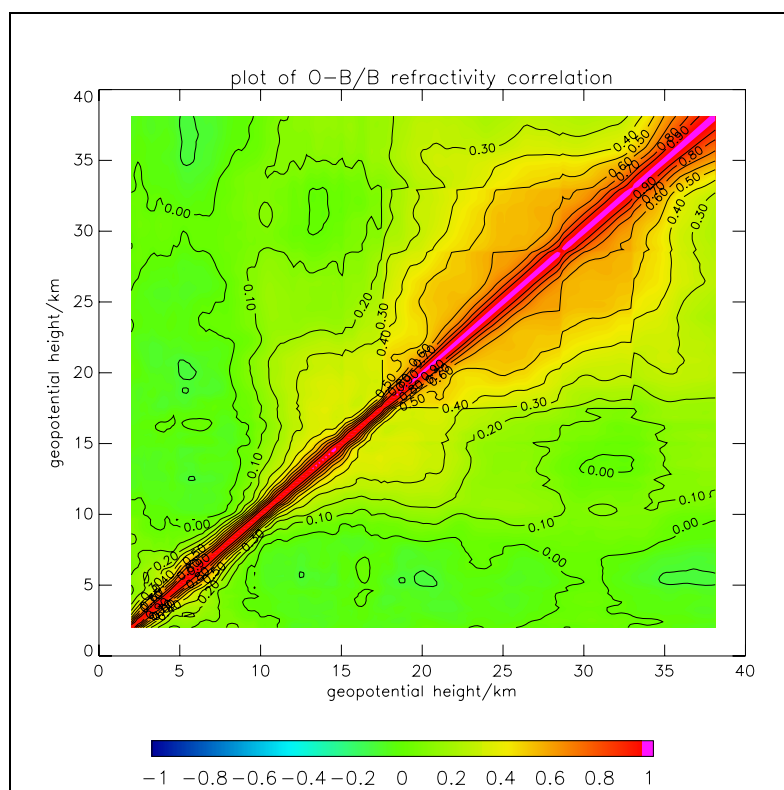


**Figure 11.** Plot of the vertical correlation in refractivity (O-B)/B. This is using UCAR processed CHAMP data for the period 7 September till 8 October 2007.

## 4. Experimental Set-up

### *a. Global model*

The Met Office global model is currently run at N320 L50, that is it has a horizontal resolution of 640 (320x2) grid points round the globe (east-west) and 481 (320x1.5) grid points (north-south), approximately 40 km at mid-latitudes, and a vertical resolution of 50 levels with model top ~63 km (~0.1 hPa). An upgrade to 70 levels up to 80 km is planned for the near future.

The Met Office global analyses are formed using 4D-Var which was introduced in 2004; see Rawlins et al. (2006). The operational NWP system generates a global analysis every six hours (at 0, 6, 12 and 18 GMT) using the 4D-Var scheme with each cycle having an assimilation time window of 6 hours centred on the analysis time. Each analysis (i.e. QG00, QG06, QG12 and QG18) uses a six hour forecast as the background from an update run of the previous analysis (e.g. QG12 will use a 6 hour forecast from QU06 as background), the update run allows nearly all the observations from the 6 hour window of the previous analysis to be used (since the time cut-off is ~ 6 hours after analysis time), whereas the QG runs currently have a time cut-off about 2 hours 47 minutes after the analysis time. From the QG00 and QG12 analyses forecasts out to seven days are produced and from QG06 and QG18 forecasts out to two days are produced. In trials only forecasts ran from the QG12 out to six days are used for verification.

For the GPS RO forecast impact experiments the control and experiment runs of the NWP system were closely based on the operational suite with the notable exception that the forecasts were run at a lower horizontal resolution. The forecasts were run at N216 L50 i.e. 432 by 325 grid points and 50 vertical levels. This was chosen in order to reduce computational time. The horizontal resolution of the model is still significantly better than the horizontal resolution of GPS RO ~300 km. However, the vertical resolution of GPS RO is higher than the model in the vertical ranges of interest (At 10 km, vertical resolution < 1 km for GPS RO compared to ~1 km for model). Consequently the GPS RO observations will contain smaller-scale vertical structures than the NWP model can resolve, potentially leading to poor fitting of the data in certain cases (e.g. gravity waves, sharp tropopause or inversions) in the resulting analyses. These representativeness errors in the forward model should be accounted for in the total error used in OPS and VAR. The model may be able to represent some of these sharp vertical features however prior to GPS RO very little data was available which such good resolution in the upper troposphere/lower stratosphere.

### *b. Errors and altitude cut-offs*

Variational data assimilation requires an estimate of the errors in observations and the forward model; these are provided as a covariance matrix on the same vertical levels as the observation. Currently we make no distinction between receivers and processing for the errors, however this may need to be improved in future if better quality data is provided from new instruments or processing techniques e.g. GRAS could potentially have lower errors than other instruments at high altitudes due to improved SNR.

Prior to the trials described in this report we adopted an error covariance matrix similar to that suggested by Steiner et al (2005) for the CHAMP satellite. When using this matrix the VAR

statistics showed GPS RO was contributing a very large proportion of the cost function; it was larger than ATOVS and the temperature observations from radiosondes which seemed disproportionate given the quantity of ATOVS data and the quality of radiosondes. Improvements in the forecasts due to GPS RO were not large enough to justify its expense in the assimilation. This indicated that the assigned errors for GPS RO were too small and that it was forcing the assimilation to fit model levels disproportionately. In particular large analysis increments were seen in potential temperature at level 30 (~18 km), the increments were not necessary wrong but just notably large.

To combat this, errors were increased below 10 km by a factor of three (in hindsight errors should have been increased above 10 km as will be explained). This led to some improvement, however these errors below 10 km were clearly too big given that they were significantly larger than (O-B)/B standard deviation especially for higher latitude occultations (about four times too large, see blue line in Figure 12) and even in the tropics. A forecast impact experiment using a revised set of errors and including latitude dependence was run. The errors were based on the observation minus background statistics for refractivity of COSMIC data over low ( $|\text{lat}| \leq 30^\circ$ ), middle ( $30^\circ < |\text{lat}| \leq 60^\circ$ ) and high ( $|\text{lat}| > 60^\circ$ ) latitudes (the statistics for the six satellites were very similar). In effect this brought the errors below 10 km back to more realistic values and above 10 km the errors were increased (see Figure 12).

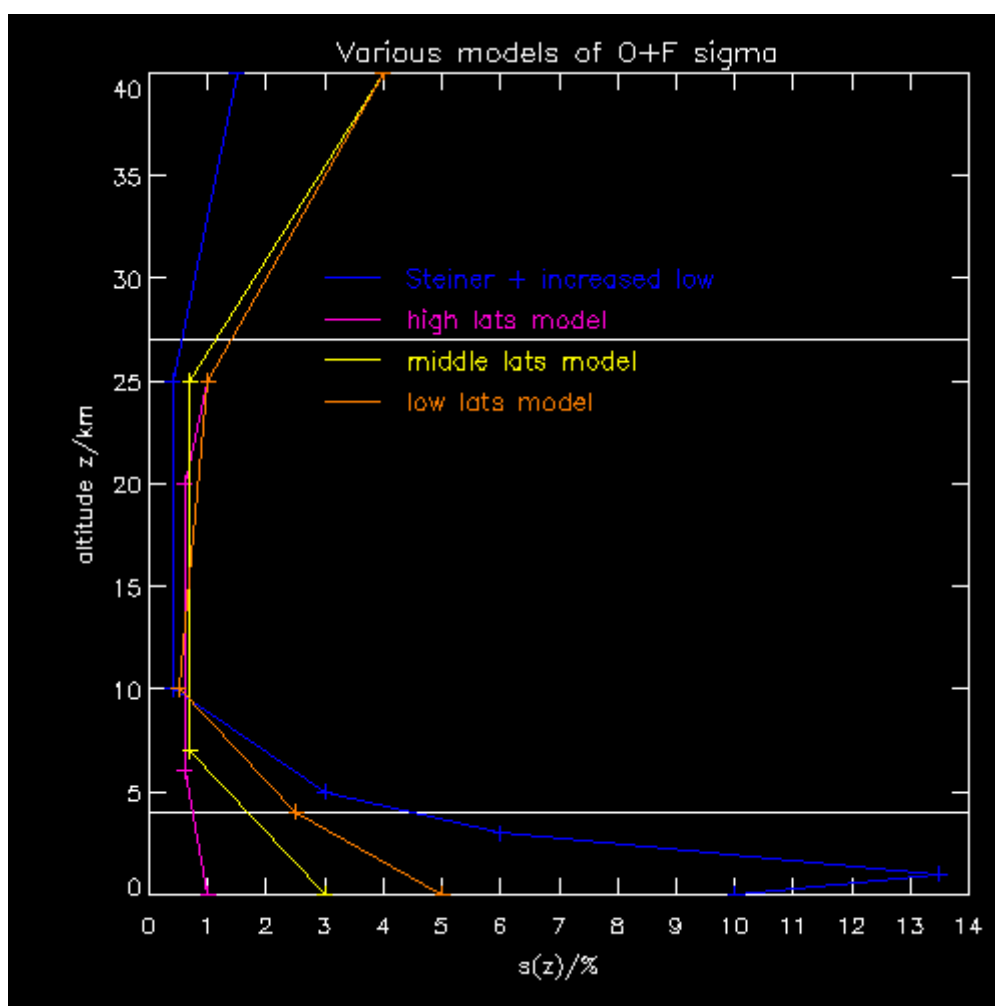


**Figure 12.** Different models of the relative error of refractivity plus forward model. The blue is the original global errors; the other colours are the three latitudinal chosen error profiles based on (O-B)/B standard deviation plots for COSMIC data.

The use of the new errors gave positive impact particularly with respect to analyses (see section 0) and the penalty in VAR was reduced by ~10%, suggesting the small increase in the errors above 10 km was very significant and GPS RO must have been over-weighted in the stratosphere. These latitude dependent errors are now being used operationally.

The error correlation model is given by a simple exponential drop-off with height difference with a constant scale height of 3.3 km throughout an occultation; an investigation into its optimisation should be done in future, unless we change to bending angle assimilation. Some idea of the observation correlation of refractivity can be gained from the vertical correlation of (O-B)/B as discussed in Monitoring Results, section 3.

Neighbouring occultations are assumed to have independent errors, but if they are sufficiently close in time and space then this assumption may be wrong. For the first few months after launch COSMIC occultations were very close in proximity due to the satellites being in similar orbits. As mentioned previously this may have led to the poor results obtained when trialling in the August 2006 period; a simple solution would be to horizontally thin the data.

This should no longer be a significant problem as the satellites are now approaching their final orbits and therefore the occultations are mostly well spread, however with the likes of GRAS being assimilated then the potential for overlapping observations still exists. Perhaps the data should be thinned in space and time to stop this possibility.

Due to known problems with negative biases in refractivity data at the bottom of the atmosphere (see Ao et al (2003) and the Monitoring Results section) and the affects of a priori climatology and noise at the top of the profiles, we decided initially to reject data below 4 km and above 27 km. However there may be some benefit, in spite of this, to using a higher cut-off to reduce model biases above 27 km (see section 5) and assimilation below 4km may provide benefit in some scenarios. The tuning of cut-offs and errors to achieve the optimal benefit is in progress.

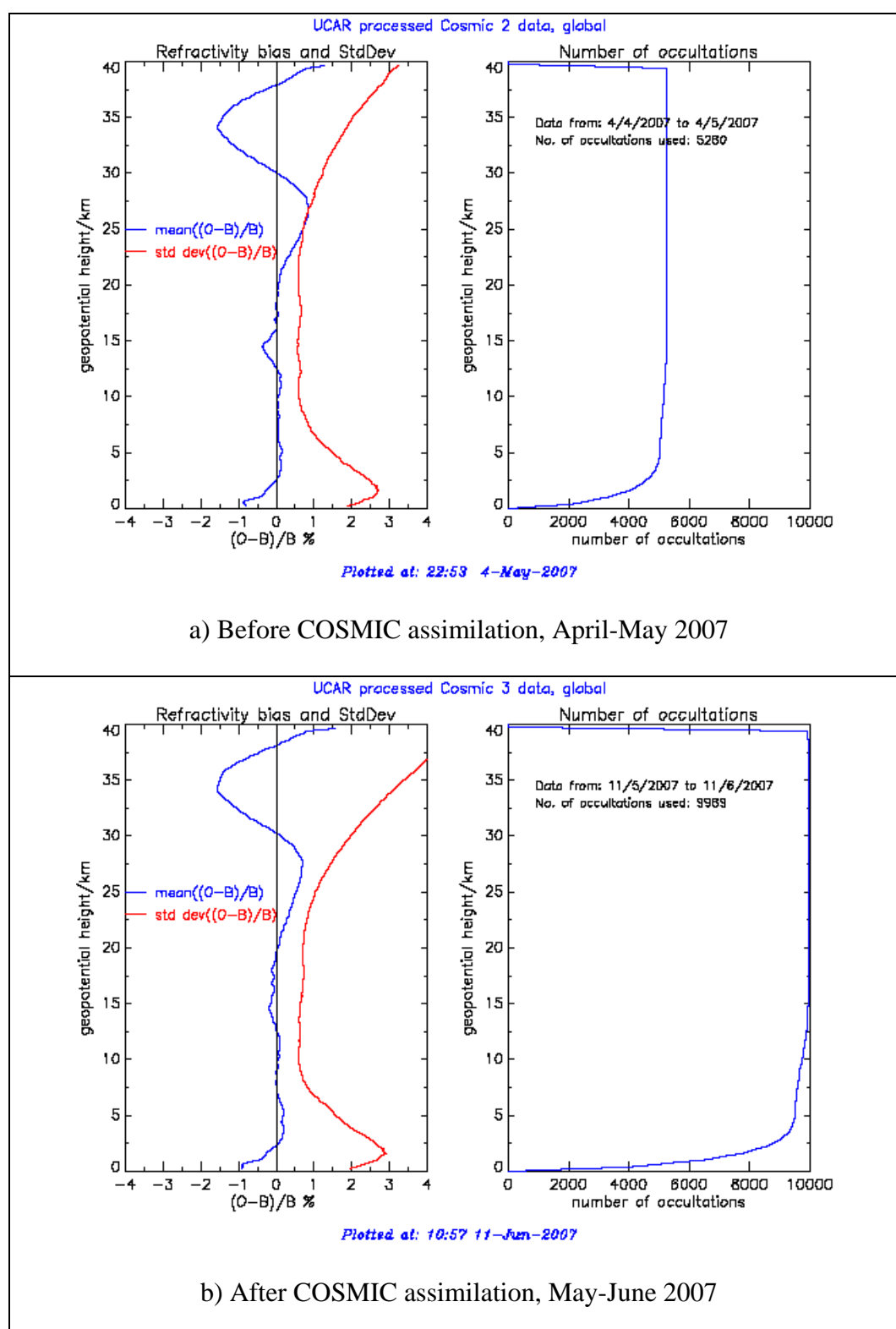


**Figure 13.** Global refractivity bias and standard deviation for satellite FM3 using one month's data. Top plot (a) is before the operational assimilation of COSMIC data and the bottom plot (b) is after the assimilation of COSMIC.



In Figure 13a which is in a period before assimilating GPS RO, one can see the ‘bump’ of negative bias at ~15 km which is associated with the low to middle latitude tropopause (see the Monitoring Results section). This is reduced after COSMIC data assimilation (see Figure 13b using a 4-27 km cut-off), also the positive bias at ~27 km is reduced a little. It is encouraging to see model biases being reduced (i.e. the GPS RO assimilation system is working as expected). Similar improvements in biases have been evident at ECMWF since they began assimilating COSMIC, especially the reduction of oscillatory biases seen over Antarctica. This bias reduction can be seen not only when comparing COSMIC data with the model (during COSMIC assimilation) but also with independent RO data which is not assimilated e.g. CHAMP from GFZ.

### *c. The experiments*

It is normal practice at the Met Office to assess the impact of a new observation type on NWP forecasts relative to the current operational NWP system and in this section we describe the experiments that were performed for GPS RO data with this in mind. Experiments were performed for two periods: 27<sup>th</sup> November until 27<sup>th</sup> December 2006 (refer to as “winter” for convenience) and 24<sup>th</sup> May until 24<sup>th</sup> June 2007 (“summer”). All observations that were used operationally during both periods were used in the experiments.

The Northern Hemisphere winter period experiments are described first. During this period only two satellites (namely FM2, FM5) were near their final orbits of above 800 km. As previously mentioned, problems may arise in the 4D-Var system when occultations are very close in location and time since error correlations between occultations are not taken into account and we may force the analyses too hard, this was kept in mind for these experiments.

Over this “winter” period five experiments were run. One included all six satellites (COSMICx6), a second (COSMICx4) used only the four most widely spread satellites (FM2, 3, 5 and 6); comparing the results of these two experiments gave insights into the influence of extra data. The impact from the use of extra data provides information on how saturated the system is with GPS RO data. A third experiment (LatR) tested the impact of the latitude dependent R matrices compared to a previously used global **R** matrix (see Figure 12), both experiment and control used all 6 COSMIC satellites. The fourth and fifth experiments tested using no lower cut-off (No\_low) and no upper cut-off (No\_upper) respectively with both using the latitude dependent errors. Figure 14a shows the number occultations used in the COSMICx4 and COSMICx6 trials (and hence the numbers used in the LatR, No\_low and No\_upper trials).

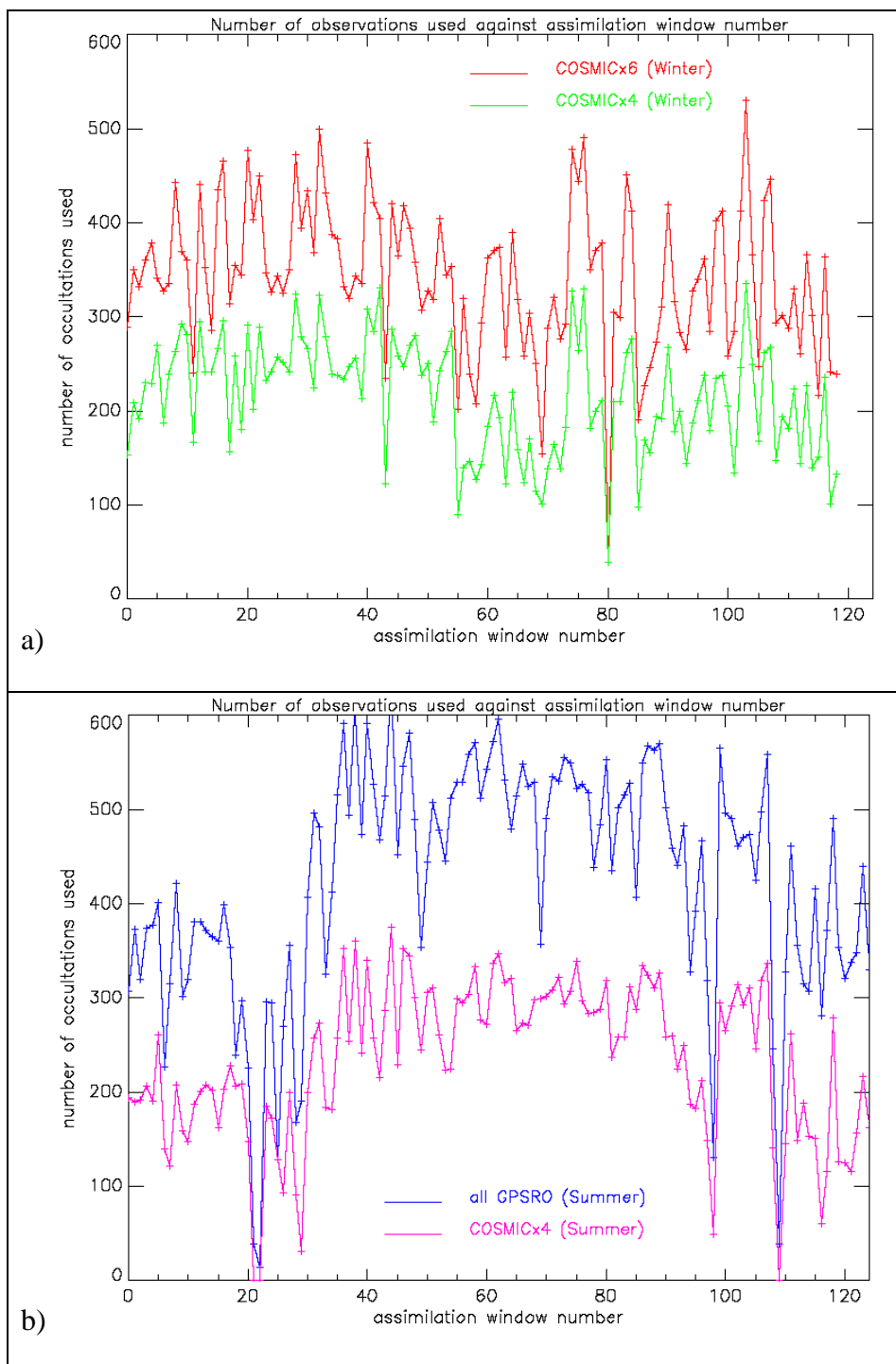


**Figure 14.** Plot of the number of occultations used in the update runs in the a) “winter” trials and b) “summer” trials as a function of assimilation window number i.e. every 6 hours.

Now we will describe the Northern Hemisphere Summer period trials or “summer”. During this period the COSMIC satellites had a greater orbital spread than in “winter”. In this period CHAMP and GRACE-A occultation data were provided with good quality and timeliness,

therefore it was decided to run a trial using all the available GPS RO data (All\_GPSRO i.e. eight receivers) compared to no GPS RO data (no\_GPSRO). A second experiment with only the 4 COSMIC satellites (4xCOSMIC) as used in “winter” was also run to see the effect of using less data, see Figure 14b. A feature worth noting in the “summer” period is that on several cycles the number of occultations dropped close to zero. Experimentation with altering the cut-off heights was also conducted: a trial was run with a 0-40 km cut-off (0-40km\_cut-off) and a 0-27 km cut-off (0-27km\_cut-off). A summary of the trials for both periods is given below in Table 1.

**Table 1** Summary of the trials

<b>Name of trial</b>	<b>Control</b>	<b>Experiment</b>	<b>Period</b>	<b>GPSRO R matrix</b>	<b>Vertical cut-offs/km</b>
COSMICx4	No GPSRO assimilated	4 COSMIC sats assimilated	winter	Old global	4-27
COSMICx6	No GPSRO assimilated	6 COSMIC sats assimilated	winter	Old global	4-27
latR	6 COSMIC sats assimilated	6 COSMIC sats assimilated	winter	Old global (control) Latitude varying (exp)	4-27
No_low	6 COSMIC sats assimilated	6 COSMIC sats assimilated	winter	Latitude varying	4-27 (control) 0-27 (exp)
No_upper	6 COSMIC sats assimilated	6 COSMIC sats assimilated	winter	Latitude varying	4-27 (control) 4-40 (exp)
COSMICx4	No GPSRO assimilated	4 COSMIC sats assimilated	summer	Latitude varying	4-27
All_GPSRO	No GPSRO assimilated	6 COSMIC sats + CHAMP + GRACE-A assimilated	summer	Latitude varying	4-27
0-40km_cut-off	6 COSMIC sats + CHAMP + GRACE-A assimilated	6 COSMIC sats + CHAMP + GRACE-A assimilated	summer	Latitude varying	4-27 (control) 0-40 (exp)
0-27km_cut-off	6 COSMIC sats + CHAMP + GRACE-A assimilated	6 COSMIC sats + CHAMP + GRACE-A assimilated	summer	Latitude varying	4-27 (control) 0-27 (exp)

## 5. Forecast Impact Trials

### a. Analysis Increments

An initial look at the effect of the GPS RO observations on an analysis can be made by comparing the analysis increments with and without GPS RO. An analysis increment is the difference between an analysis and a corresponding background. If one subtracts the analysis increments of the control from those of the experiment then one can see the difference made by GPS RO observations. An example of this is shown from the “winter” COSMICx6 experiment in Figure 15 for 12 UTC analysis time on the 20<sup>th</sup> December 2006 in the form of a map of temperature increments at pressure level 250 hPa (~12 km).

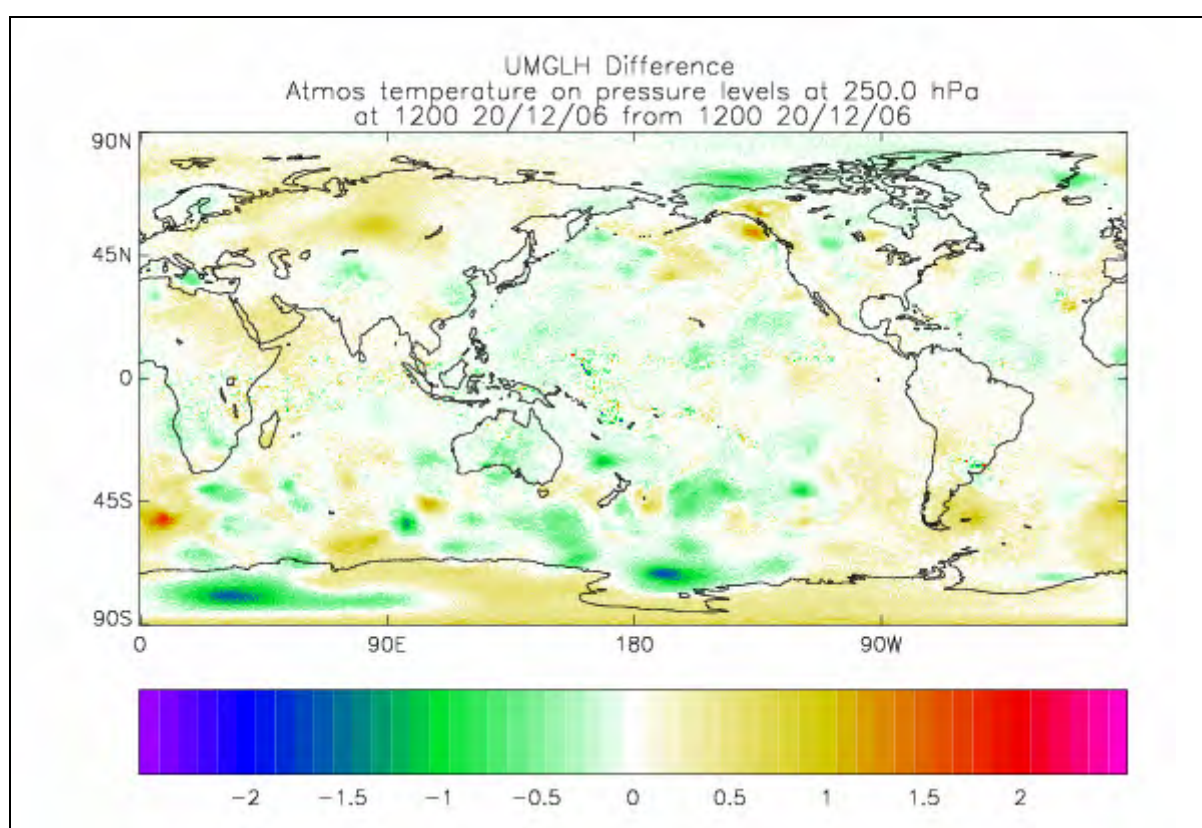


**Figure 15.** COSMICx6 result. Plot of (experiment – control) in analysis increments of temperature at 250 hPa. Scale unit: K

The most distinctive features of the plot are the patches of cooling and warming, which in this case are largest in the southern hemisphere extra tropics. These patches surround the tangent point of the responsible occultation; the **B** matrix spreads the information in the horizontal over large areas. Figure 16 displays profiles of the effect of one such occultation. It shows the same increments as shown in Figure 15 but as a vertical profile (Figure 16a) at the centre of the

cooling seen at 250 hPa in Antarctica at about 79°S latitude, 33°E longitude. Figure 16b also shows the corresponding 1D-Var result of the responsible occultation (right plot).

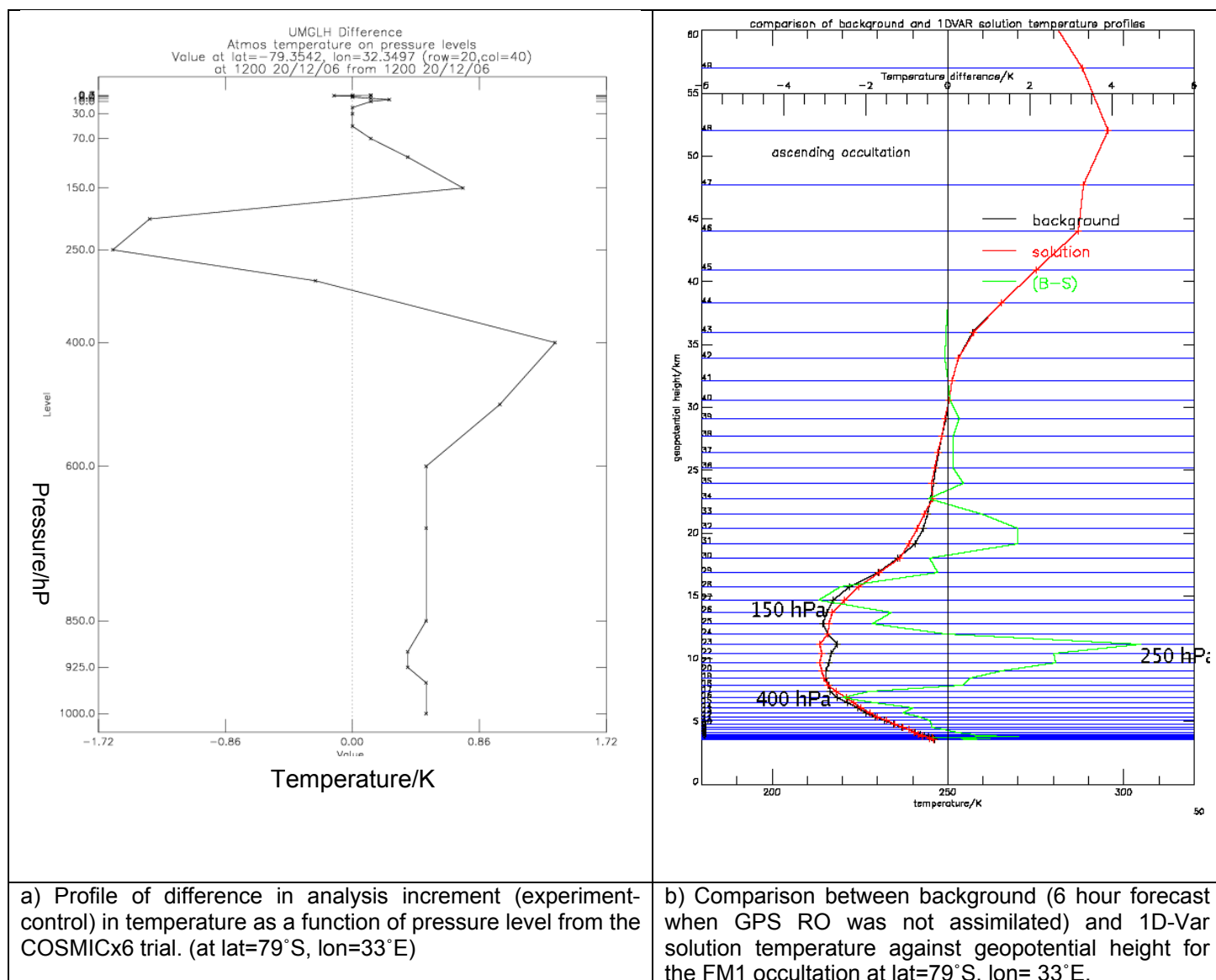
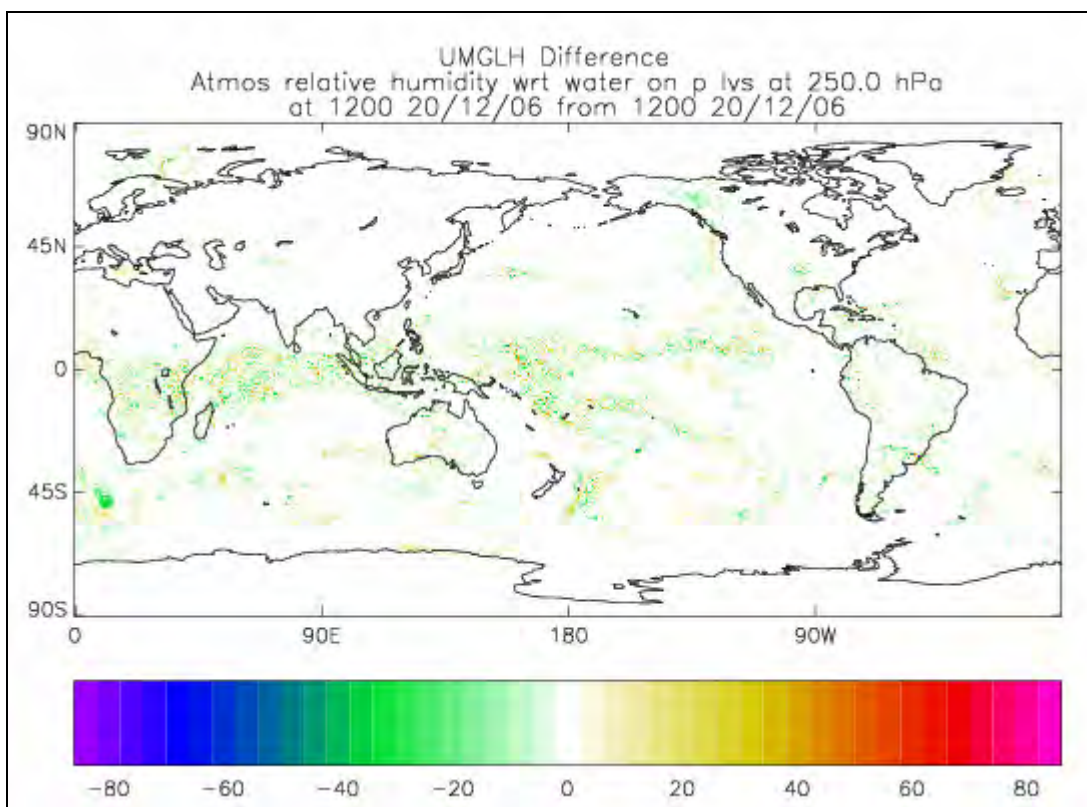


Figure 16.

Although the plots in Figure 16 show temperature on different vertical scales (16a pressure and 16b geopotential height), one can still see that the spikes in background minus 1D-Var solution (green on the right plot) match the increment difference spikes from the trial (on the left plot); note the corresponding pressures are marked on the right plot. The spikes are of the opposite sign since the left plot is (GPS RO - control) while the right is (background - GPS RO).

Therefore the 1D-Var behaviour is consistent with 4D-Var as one would expect; this was seen in many examples. Of course this does not confirm that the increments are correct; the results of forecast impact experiments will demonstrate if GPS RO is consistently producing useful increments as expressed in the improvement in the derived forecasts.

The increments observed in relative humidity are more subtle than temperature (especially high up at 250 hPa) and are less obviously associated with individual occultations; however the increment patch (Figure 17) south-west of South Africa is at the same horizontal position as the temperature increment in Figure 15. This is associated with a FM6 occultation that led to a sharpening of the tropopause at ~200 hPa (cooling) and slight warming at 250 hPa.

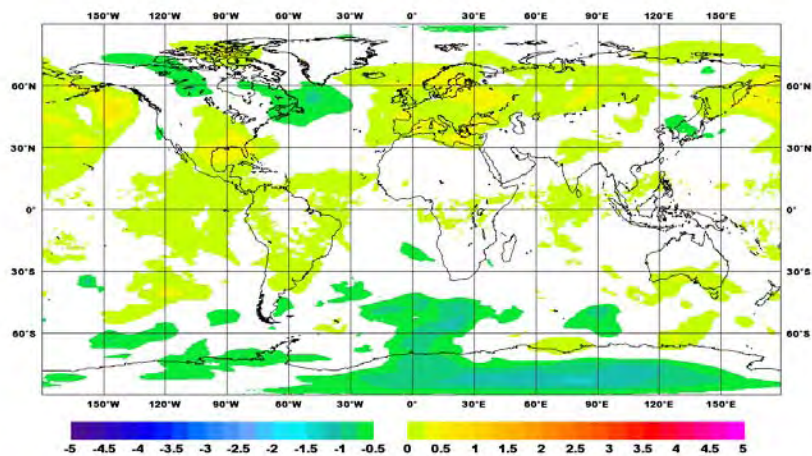


**Figure 17.** COSMICx6 result. Plot of (experiment – control) in analysis increments of relative humidity at 250 hPa. Scale: %

Figure 18 shows the 250 hPa temperature differences between the monthly average fields of the COSMICx6 experiment and control (no GPS RO). One can see that patterns exhibited at analysis (plot a) are still evident at different forecast ranges (b, c and d). One noticeable feature is the patch of cooling evident over Antarctica (which is consistent with the behaviour shown in Figure 16 associated with a cooling at the tropopause at these high latitudes).

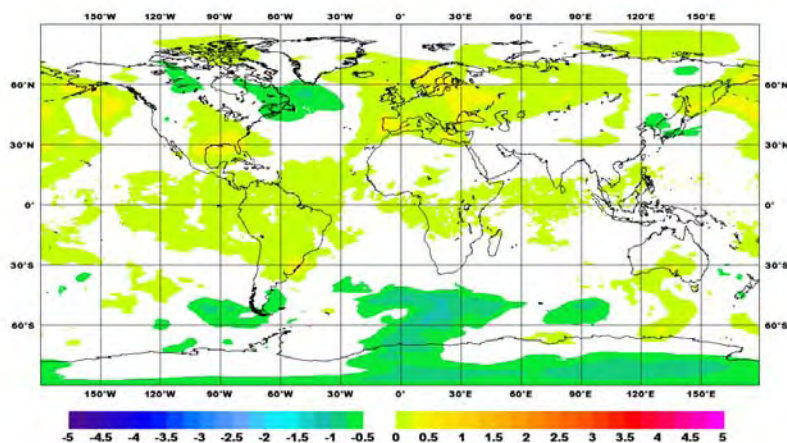


**Mean Field : Verifying Analysis, T+24**  
**TEMPERATURE (K) at 250hPa**  
 min: -1.3 max: 0.71 mean: -0.12 RMS: 0.26 SD: 0.23

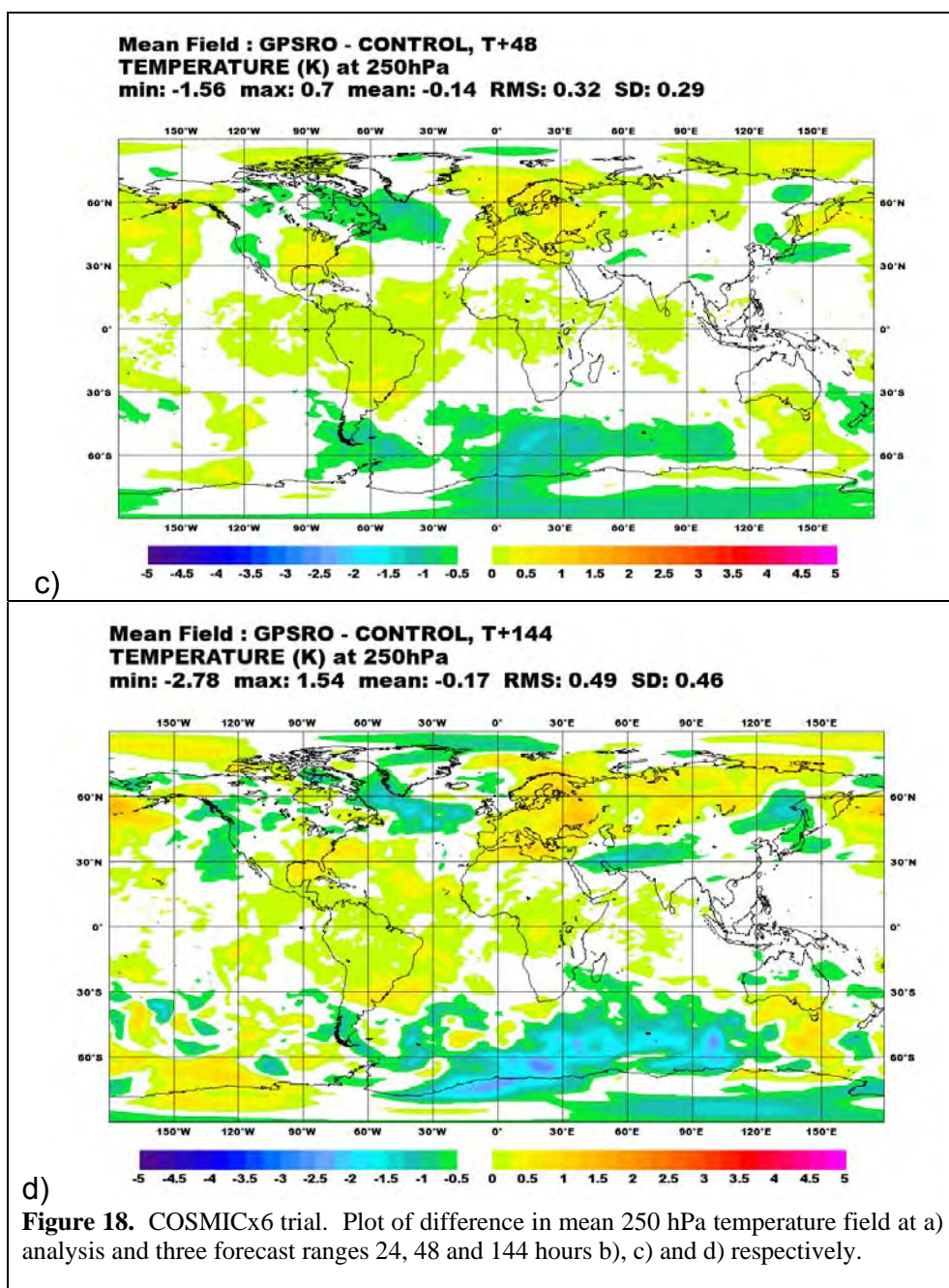


a)

**Mean Field : GPSRO - CONTROL, T+24**  
**TEMPERATURE (K) at 250hPa**  
 min: -1.21 max: 0.51 mean: -0.11 RMS: 0.25 SD: 0.22



b)



A distinctive feature of the “summer” trials was GPS RO’s influence on the 100 hPa temperature fields in the tropics and a corresponding change in the wind fields at 100 hPa, see Figure 19. This region is known to have been convectively active at the time of the trial. 100 hPa (~17 km) is around the height of the tropical tropopause. Perhaps the change at the tropopause is altering the stability of the atmosphere which will affect convection hence influencing the Hadley cell circulation and the winds.



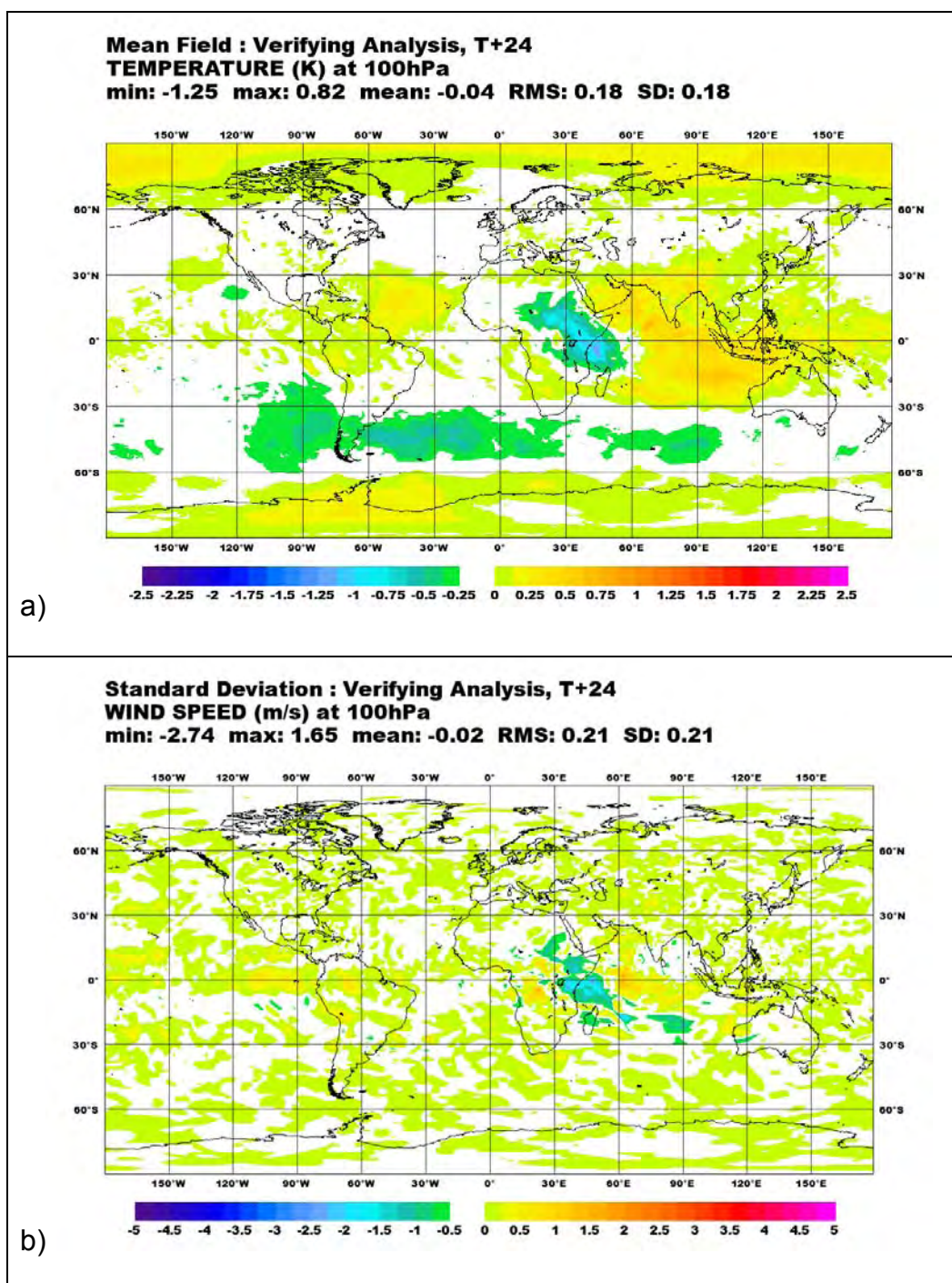


**Figure 19.** All\_GPSRO trial results: the difference of the mean fields for the “summer” period between trial (All\_GPSRO) and control (no GPSRO) for a) 100 hPa temperature at analysis and b) wind speed field at analysis.

An interesting feature of the trials results were the average changes made to the pressure on ‘rho’ model levels, see Figure 20, note pressure is a variable in the GPS RO state vector in VAR. Notice that in the “winter” period (Figure 20a.) there are large features below model level

~25 but only over the high latitudes and that the northern hemisphere has the largest features. One might expect this in that the trial period is for the northern hemisphere winter, where the atmosphere is more active and potentially there are more features of the analysis to adjust. In the “summer” period (Figure 20b.), the magnitude of the features are much smaller (note the change of scale), this is probably partly due to the observation errors being larger for GPS RO in the All\_GPSRO trial compared to the COSMICx6 trial. One feature in common is that the largest features are again over the high latitudes and that these are greatest over the winter pole.

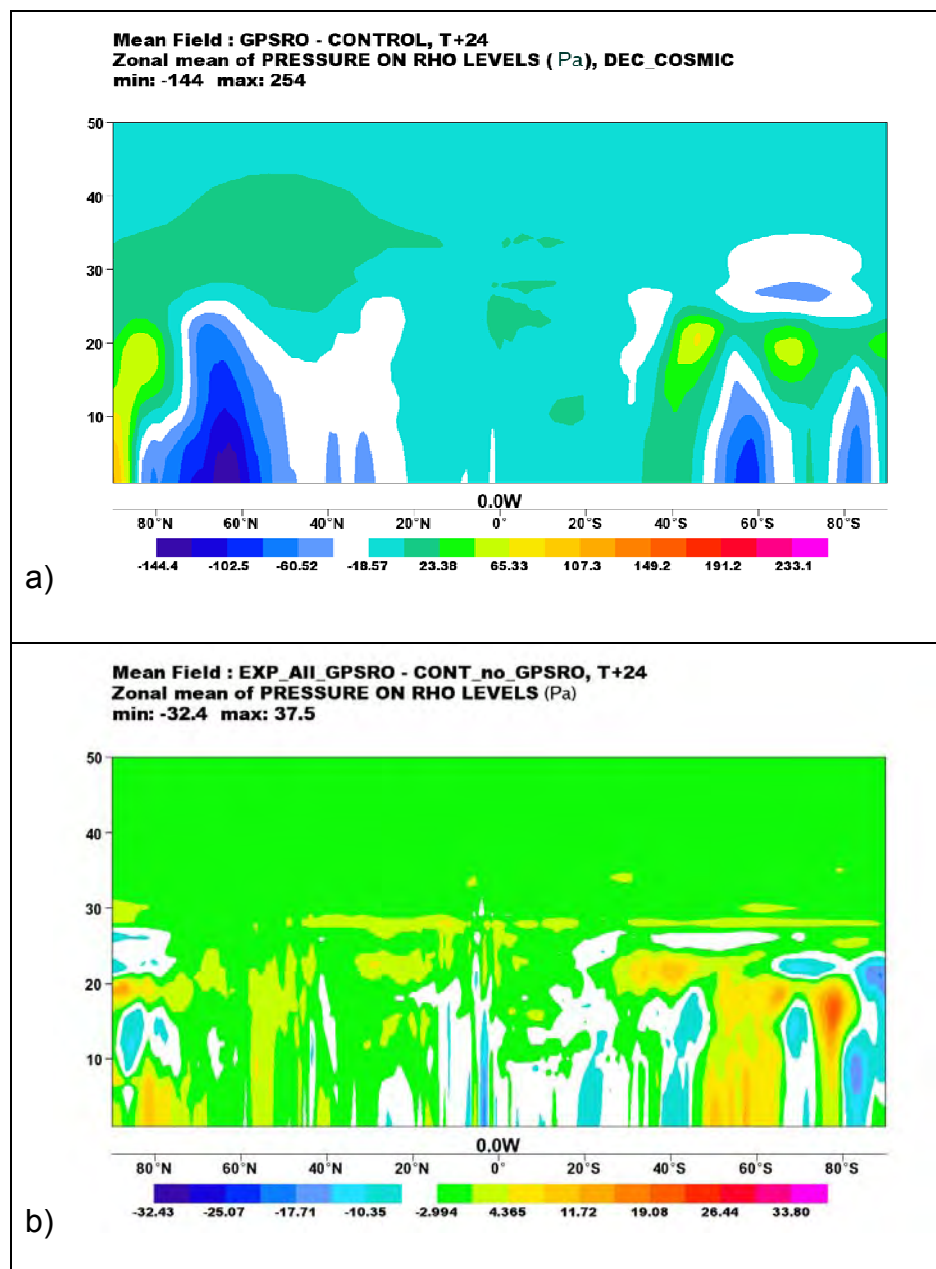


**Figure 20.** a) “winter” COSMICx6 trial result, b) “summer” All\_GPSRO result. Plot of difference in mean zonal pressure of experiment and control on model levels at 24 hours forecast range.

*b. Impact on global forecasts*

The quality of the forecasts (from the UM) initialised from the control and experiment analyses for the trials were objectively assessed by calculating their differences from in situ observations such as radiosondes and land/sea surface data and also the corresponding analyses valid at the forecast time. A variable of interest is verified by comparing each forecast in the trial period with the observations (or analysis) valid at the time of the forecast and then deriving the bias and RMS difference between the observation (or analysis) and the forecast for different areas of the Earth. Variables relevant to GPS RO such as temperature, geopotential height, relative humidity were paid the most attention and to a lesser extent wind speed and surface pressure.

The results are presented for three latitude bands. The bands consist of the Northern Hemisphere extratropics (refer to as NH) and Southern Hemisphere extratropics (SH), in each case areas pole-ward of 20° and the Tropics (20°S to 20°N, TR), note these are the definitions that will be used when referring to the results. A full break-down of the changes in RMS is provided by the verification software at the Met Office: RMS changes are provided for combinations of variables and forecast times, e.g. NH relative humidity at 500 hPa with forecast range 48 hours or TR geopotential height at 50 hPa with forecast range 144 hours etc. All the combinations give a total 369 components on which to gauge forecast skill. Each component is marked as either a significant improvement i.e. 2% or more decrease in RMS of experiment compared to control (green in Table 2 and Table 3), a neutral effect i.e. 2% increase to 2% decrease (black in Table 2 and Table 3) and significantly worse i.e. 2% or more increase in RMS (red in Table 2 and Table 3). These assessments can be seen on rows four (against observations) and six (against analysis) in the summary tables.

Shown in the second and fourth rows of the summary tables are the NWP index changes for observations and analysis respectively. The NWP index is a score based on relatively few of the components which are then weighted according to what is seen to be important to Met Office customers e.g. NH winds at 250 hPa at 24 hour forecast range are weighted highest.

**Table 2** Summary of the results from the five “winter” experiments

<b>Experiment name</b>	<b>COSMICx4</b>	<b>COSMICx6</b>	<b>latR</b>	<b>No_low</b>	<b>No_upper</b>
<b>Control</b>	No GPSRO	No GPSRO	6 COSMIC global R	4-27 km cut-off	4-27 km cut-off
<b>NWP index against obs.</b>	+0.2%	+0.4%	+0.2%	+0.3%	+0.2%
<b>Forecast RMS diff. against obs.</b>	12% 88% 0%	21% 79% 0%	7% 92% 1%	4% 96% 0%	0% 100% 0%
<b>NWP index against analysis</b>	+0.25%	0.0%	+0.7%	+0.1%	0.0%
<b>Forecast RMS diff. against analysis</b>	13% 82% 5%	17% 74% 9%	19% 81% 0%	1% 98% 1%	0% 100% 0%

A summary of the results from the “winter” experiments is given in Table 2. The forecast RMS with respect to observations (fourth row down) is improved significantly in 12% of the 369 components for COSMICx4 which increases to 21% of components for COSMICx6, so using the remaining two satellites proved to be very useful, this hints that the model was far from saturated with GPS RO data. The vast majority of the improvements were in the SH e.g. for COSMICx6 (compared to observations) 62 out of the 76 improvements were in the SH. Note none of the components were made significantly worse in COSMICx4 and COSMICx6 with respect to observations. Adding latitude dependent R matrices (latR) added an extra 7% to the improvement count compared to the old errors (against observations) and significantly improved the score against analyses (19% improved).

Regarding NWP index scores, we can see that COSMIC data improved the score in all cases against observations, most significantly using the combination of all six satellites and the new errors. The largest component to the COSMICx6 NWP index score against observations was the tropical winds at 250 hPa. We can estimate latR compared to no GPS RO should give approximately 0.4+0.2% (i.e. ~+0.6%) with respect to observations (this comparison was not done directly since the versions of OPS and VAR were different for latR and the no GPS RO control).

With respect to analyses (i.e. verifying against the analysis valid at the forecast time) the trend is less clear since adding the extra two satellites led to a reduction in NWP index (from +0.25 to 0.0%) but improved the good RMS scores (17% improved for COSMICx6 compared to 13% COSMICx4), however the percentage of worse RMS scores increased by 4% with the addition. This may be a result of the analyses over-fitting GPS RO data (made worse due to the close proximity of the occultations when all six were used), the fact that the analysis NWP score improves by 0.7% when the new errors (latR, less weight in stratosphere) are used corroborates with this idea. This latR analysis improvement was obtained by an accumulation of small improvements in most fields.

A useful increase to the NWP index against observations (+0.3%) can be seen in No\_low although only a few of the components, 4%, are improved significantly. We can infer that No\_low should then give around  $0.6+0.3\%$  (i.e.  $\sim +0.9\%$ ) for the NWP index against observations compared to no GPSRO. We expect that better impact can be obtained by using a variable rather than fixed lower cut-off with the aim of rejecting the known negative biases at the bottom of the atmosphere associated with sharp vertical gradients of refractivity. The variable cut-off could perhaps be based on the background specific humidity field or the vertical gradient of background refractivity (see Figure 4).

No\_upper gave a modest improvement in NWP index (+0.2%) with respect to observations (due to PMSL and low level wind improvements) and was neutral against analyses; however no components were significantly improved or degraded. This is mostly due to the lack of verification made on components above 50 hPa or  $\sim 21$  km. Assuming the effects are additive then one can estimate for the NWP index that during this period COSMIC with a 0-40 km cut-off and using latR errors provides  $(0.4+0.2+0.3+0.2)$  i.e.  $\sim +1.1\%$  against observations and  $(0.7+0.1)$  i.e.  $\sim +0.8\%$  against analysis compared to a no GPS RO control.

We have observed biases for refractivity between different processing centres that becomes increasingly large with heights over 25 km (see Figure 8). Despite this processing bias there is still potential for removing the 'S' shaped model bias (as seen in section 3) using refractivity above the current upper cut-off of 27 km, since the model bias is larger in magnitude than the processing bias. This improvement in the bias can be seen in from the "summer" trial period in Figure 21: one can see that the high level 'S' shape bias (between 30 and 40 km) is reduced going from a) to b), this is most evident in the SH. This improvement is shown in bending angle space (when we were assimilating refractivity) which suffers less from processing biases and therefore we can be more confident in using refractivity up to 40 km.



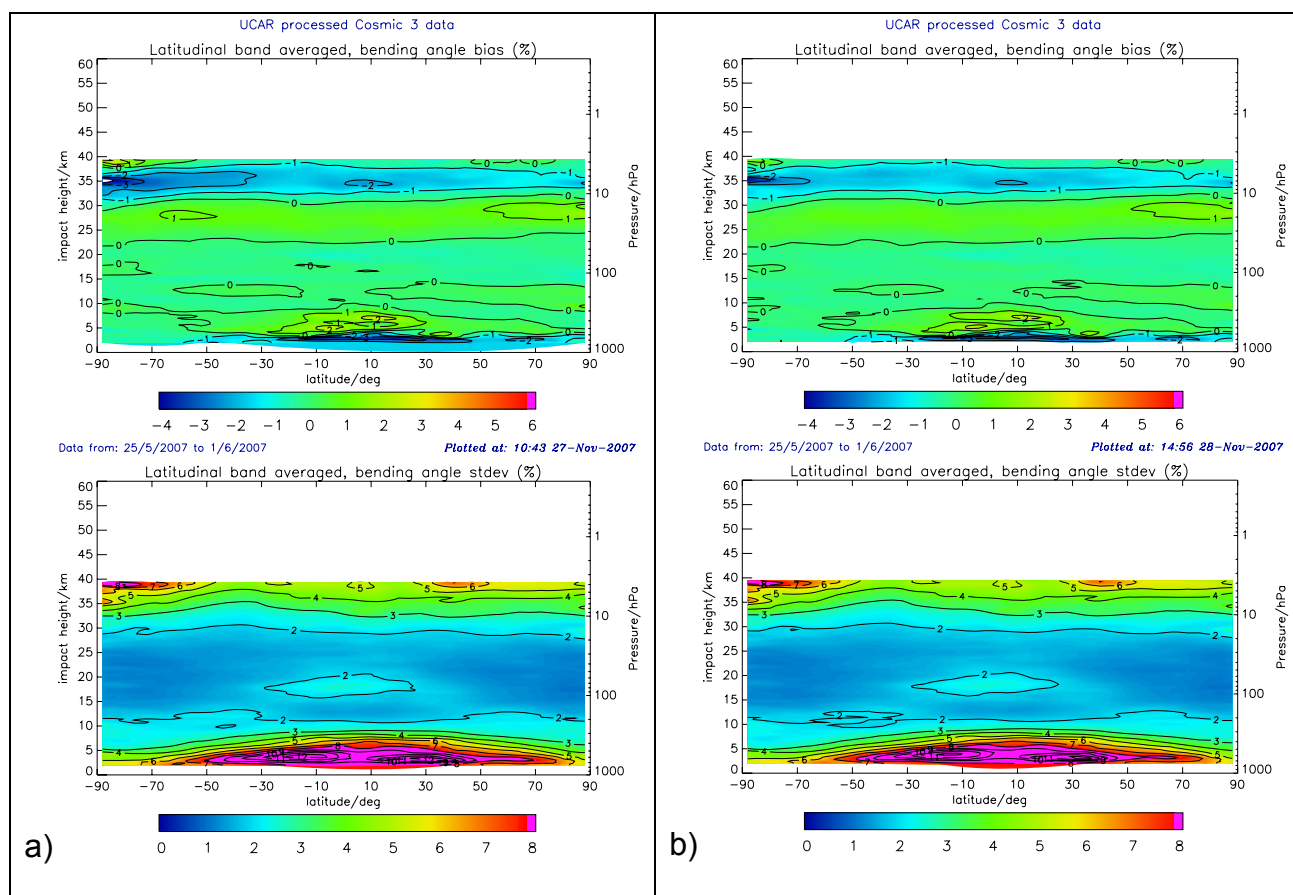


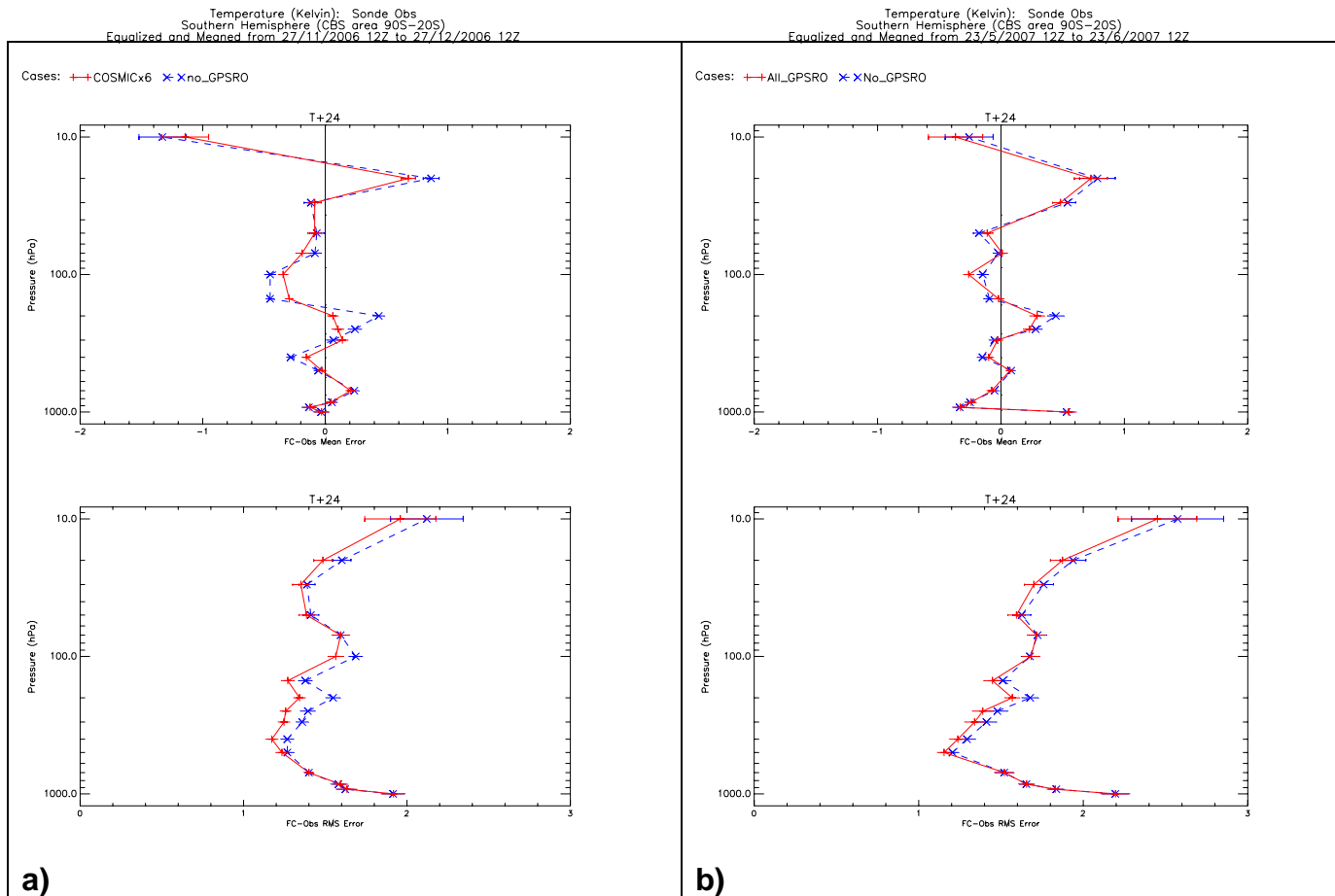
**Figure 21.** Zonally averaged bending angle (O-B)/B plots generated from a) the 6 hour forecasts from the “summer” no GPS RO control and b) the 6 hour forecasts from the “summer” 0-40 km cut-off trial (using all available GPS RO). The observations were from FM3, which was assimilated in b).

**Table 3.** Summary of the results from the “summer” experiments

<b>Experiment name</b>	<b>COSMICx4</b>	<b>All_GPSRO</b>	<b>0-40km_cut-off</b>	<b>0-27km_cut-off</b>
<b>Control</b>	No GPSRO	No GPSRO	4-27 km cut-off	4-27 km cut-off
<b>NWP index against obs.</b>	+0.4%	+0.5%	+0.4%	+0.1 %
<b>Forecast RMS diff. against obs.</b>	5% 95% 0%	7% 93% 0%	0% 100% 0%	0% 100% 0%
<b>NWP index against analysis</b>	+0.2%	+0.3%	0.0%	-0.1 %
<b>Forecast RMS diff. against analysis</b>	11% 87% 2%	14% 8 % 4%	0% 98% 2%	0% 98% 2%

A summary of the results of the “summer” trials is given in Table 3 above. The magnitude of the improvement in the “summer” period is fairly disappointing in comparison to the “winter” period. Increasing the number of observations from COSMICx4 to All\_GPSRO (see Figure 14) provided only marginal benefit. As in the “winter” trial the largest contribution to the NWP index against observations was provided by the tropical winds at 250 hPa. The maximum impact can be obtained (like in “winter”) using all available satellites and a 0-40 km cut-off giving ~ +0.9% against observations and +0.3% against analysis. The analysis scores were significantly less than in “winter”. The low analysis score is partly due to a problem encountered in the control (no GPS RO) when no data assimilation was performed on one cycle; this led to a very low analysis score for that cycle, however averaged over the period of a month the effect was not too severe. It appears for “summer” that the raising of the upper cut-off gave larger positive impact than the lowering of the lower cut-off, whereas in “winter” the lowering of the lower cut-off gave greater impact.

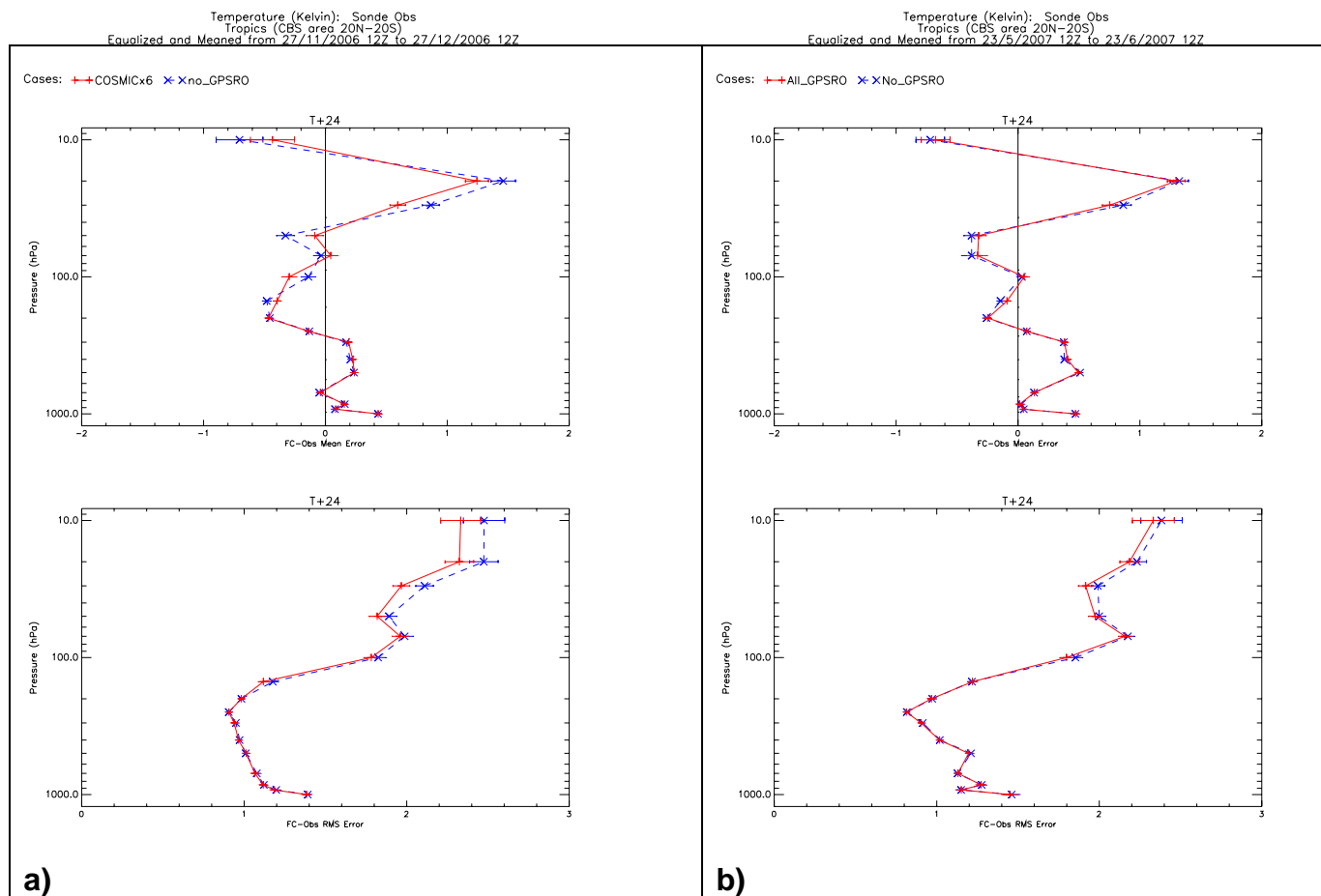
The good improvements in NWP index against observations when using a 0-40 km cut-off as seen in both seasons is mainly down to small improvements of the tropical wind fields at 850 hPa which are weighted highly because of their significance in hurricane forecasting. Generally with no lower cut-off we see very small improvements in most fields at low altitudes.



**Figure 22.** COSMICx6 “winter” trial in a) and All\_GPSRO “summer” trial result in b), both controls use no GPS RO data. Profiles of mean error (top) and RMS error (bottom) compared to radiosonde temperatures (K) at the 24 hour forecast range in the southern hemisphere. The experiments are shown in red and the controls in blue.

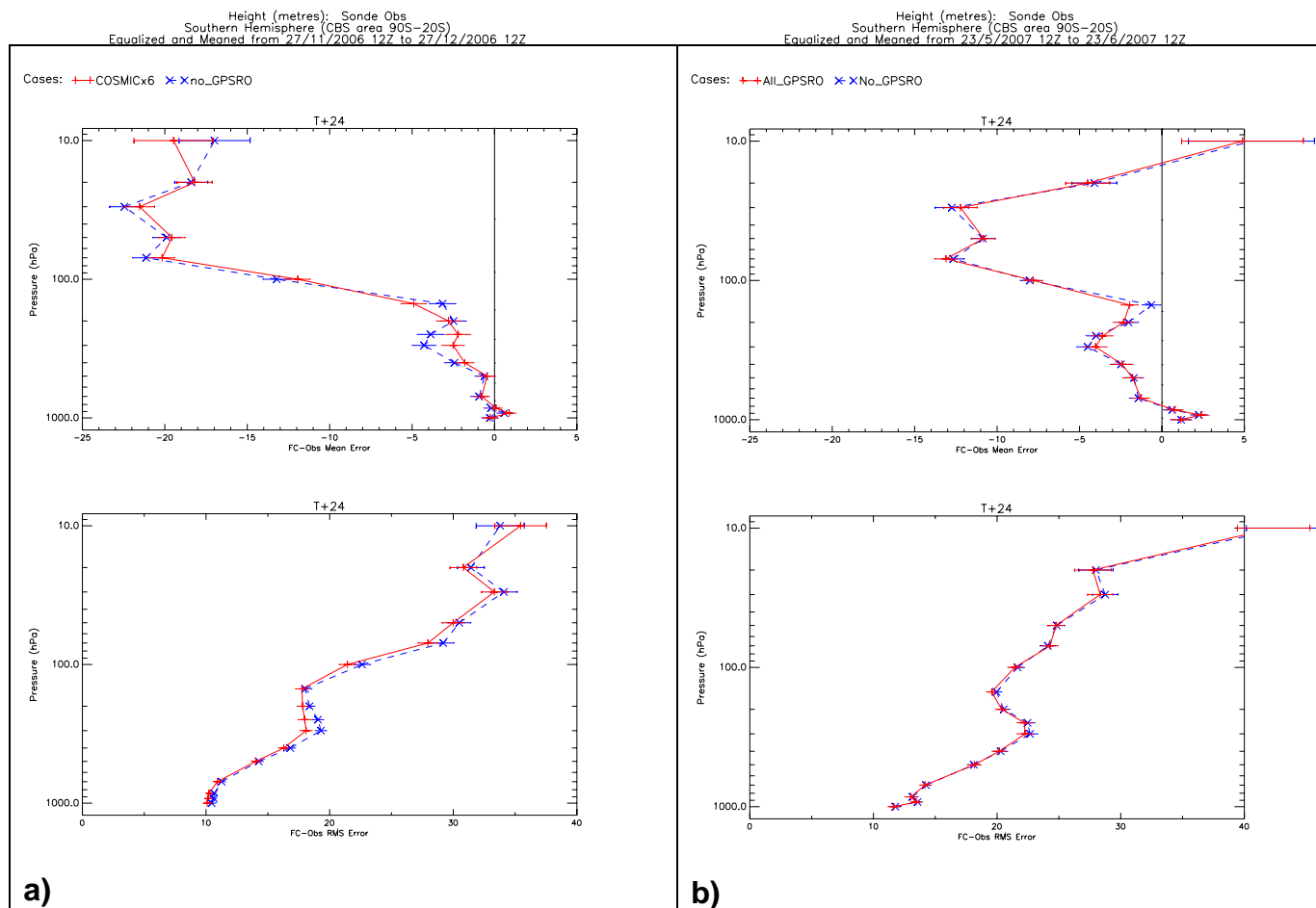
Figure 22 shows the improvement in bias and RMS compared to radiosondes for both periods of trials. We can see how GPS RO pulls the 24 hour forecasts towards the radiosonde temperatures over a wide vertical range of the atmosphere (above 500 hPa). The error bars shown in this and the following plots represent the 68% confidence interval (standard error). The “summer” period plot shows similar behaviour but with a smaller magnitude.





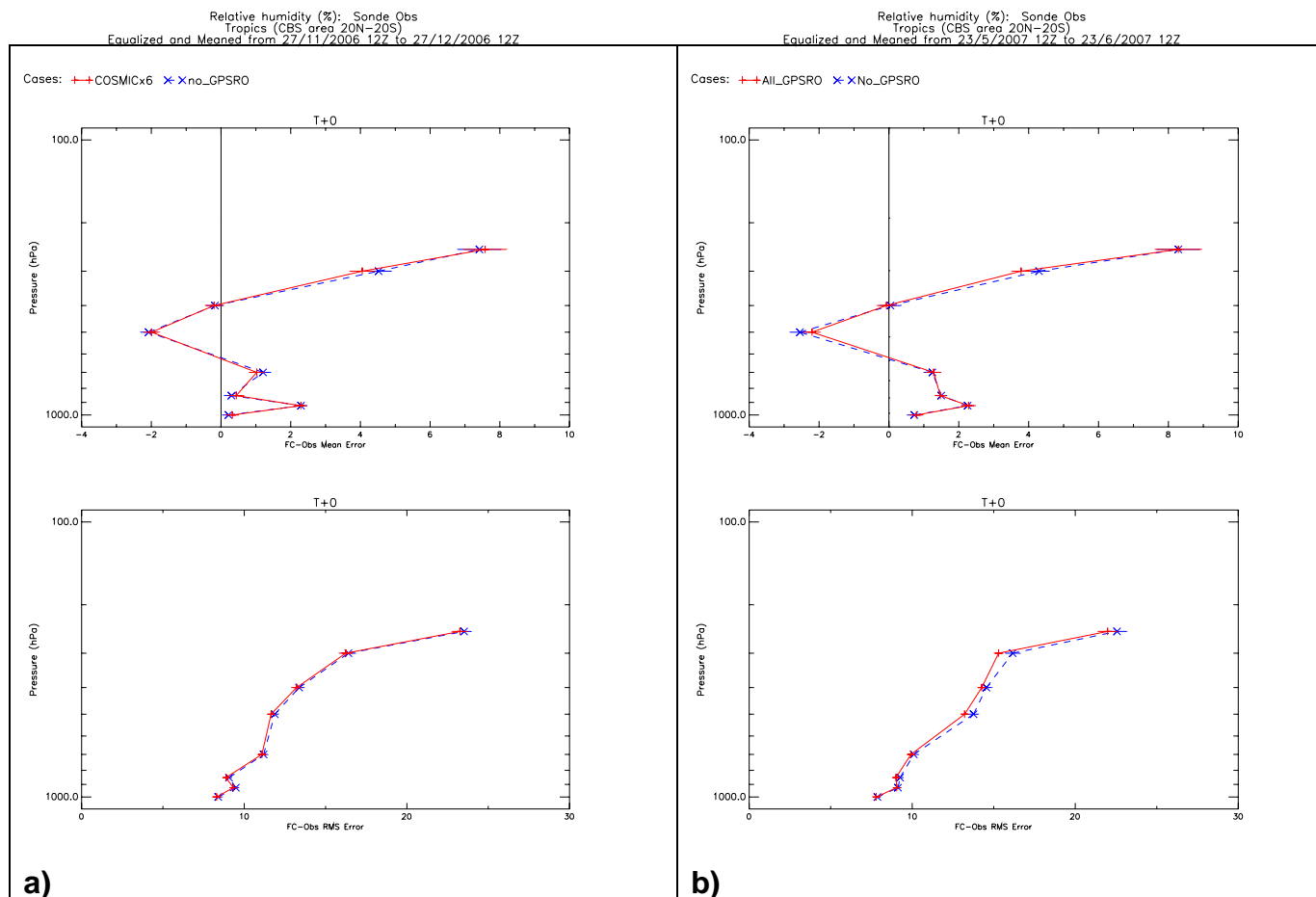
**Figure 23.** Same as Figure 22 except for Tropics.

In the tropics (Figure 23) GPS RO has a smaller impact on temperature fit to radiosondes below 100 hPa than in the SH. The impact in the NH is smaller still, as is the case for all the plots that are presented.



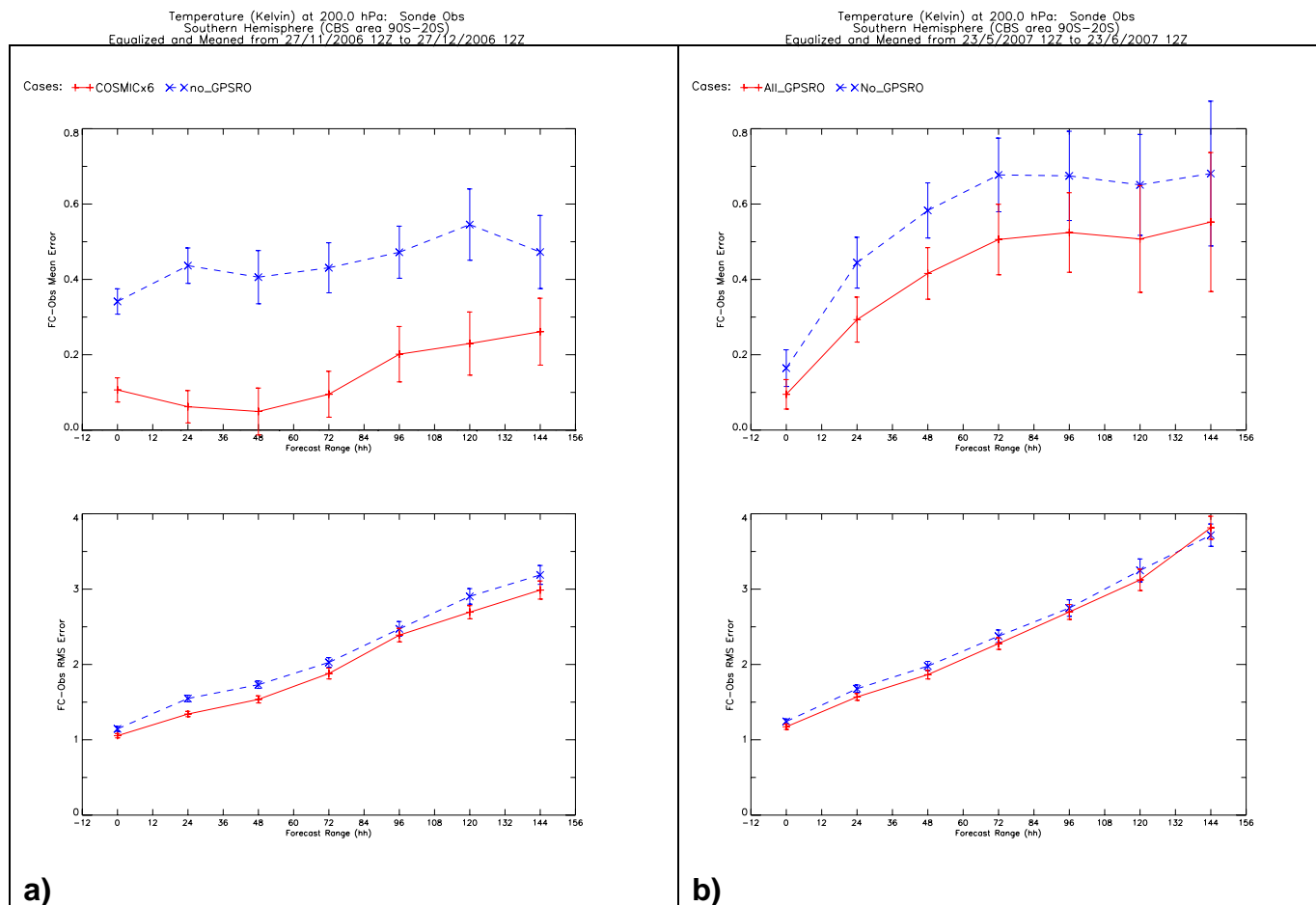
**Figure 24.** The COSMICx6 “winter” trial in a) and All\_GPSRO “summer” trial result in b). Profiles of mean error (top) and RMS error (bottom) compared to radiosonde geopotential heights (gpm) at the 24 hour forecast range in the southern hemisphere. The experiments are shown in red and the controls in blue (both with no GPS RO).

In Figure 24 one can see a good improvement in the 24 hour forecast fit to radiosonde geopotential height over a large vertical range of pressures in “winter”, however the effect is smaller in “summer”.



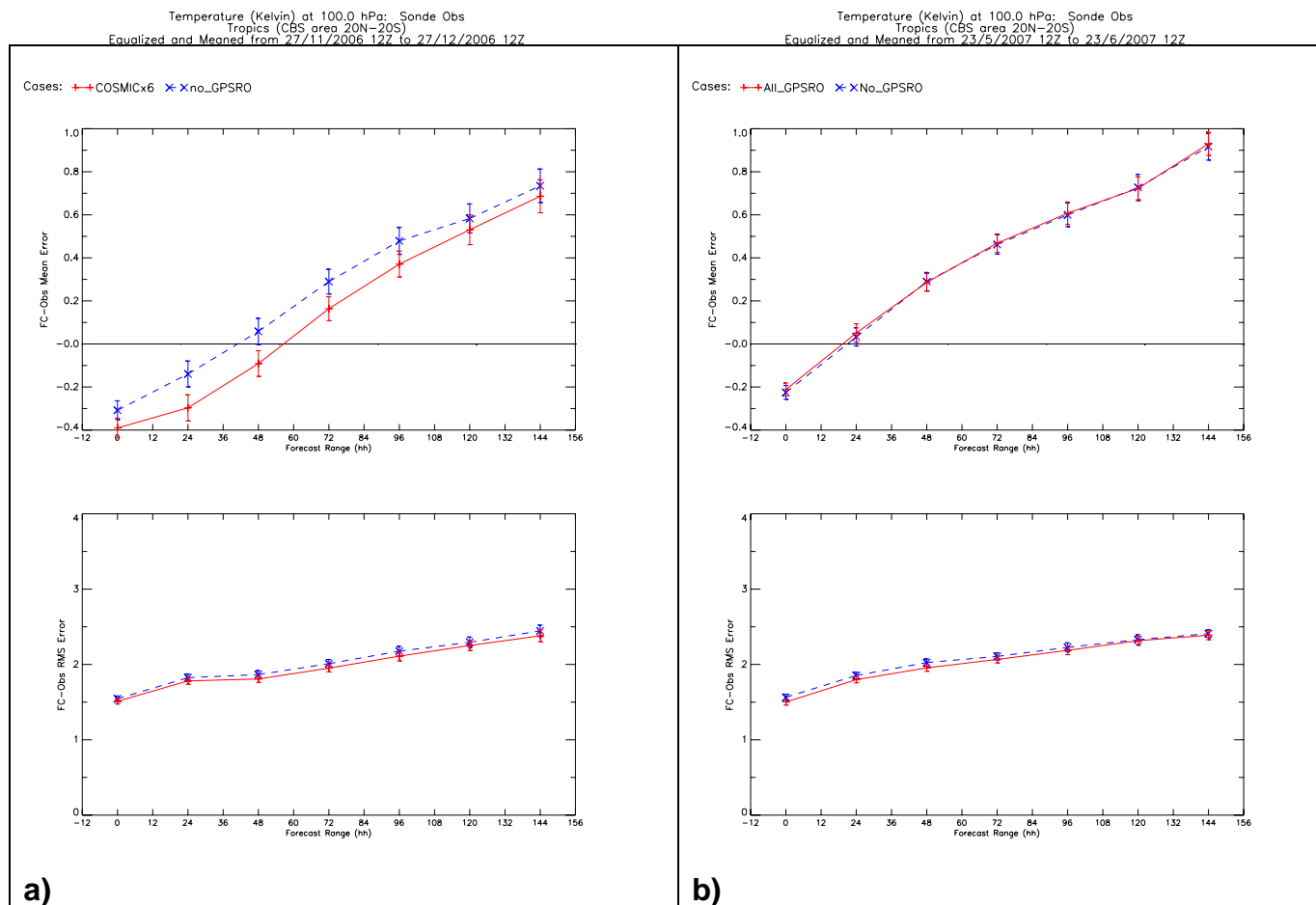
**Figure 25.** COSMICx6 “winter” trial in a) and All\_GPSRO “summer” trial result in b). Profiles of mean error (top) and RMS error (bottom) compared to radiosonde relative humidity (%) at analysis in the tropics. The experiments are shown in red and the controls in blue (both with no GPS RO).

In Figure 25 one can see a small but significant improvement in relative humidity in the TR compared to radiosondes for the “summer” period but a smaller effect for the “winter” period.



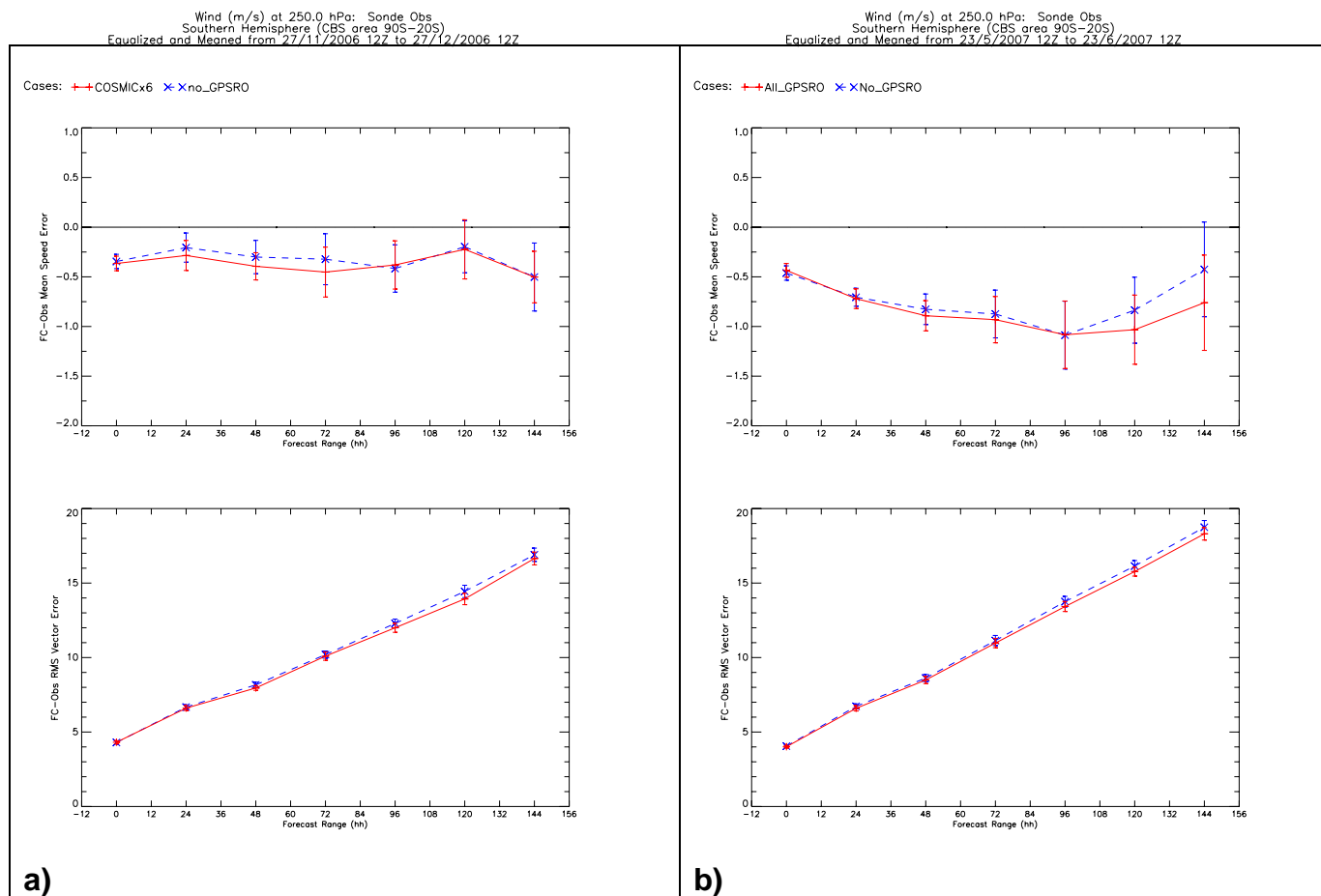
**Figure 26.** COSMICx6 “winter” trial in a) and All\_GPSRO “summer” trial result in b). Mean error (top) and RMS error (bottom) compared to radiosonde temperature (K) at 200 hPa as a function of forecast range in the southern hemisphere. The experiments are shown in red and the controls in blue (both with no GPS RO).

Perhaps the largest impact of GPS RO can be seen in Figure 26a. This shows an improvement in 200 hPa temperature bias compared to radiosondes in the SH. The bias is reduced by ~0.3 K at all forecast ranges; at analysis and the 24 hour forecast range this change is statistically significant at the 0.05 level of significance using the Student’s t-test. Similar behaviour is observed in the “summer” trial in plot b, but to a smaller magnitude.



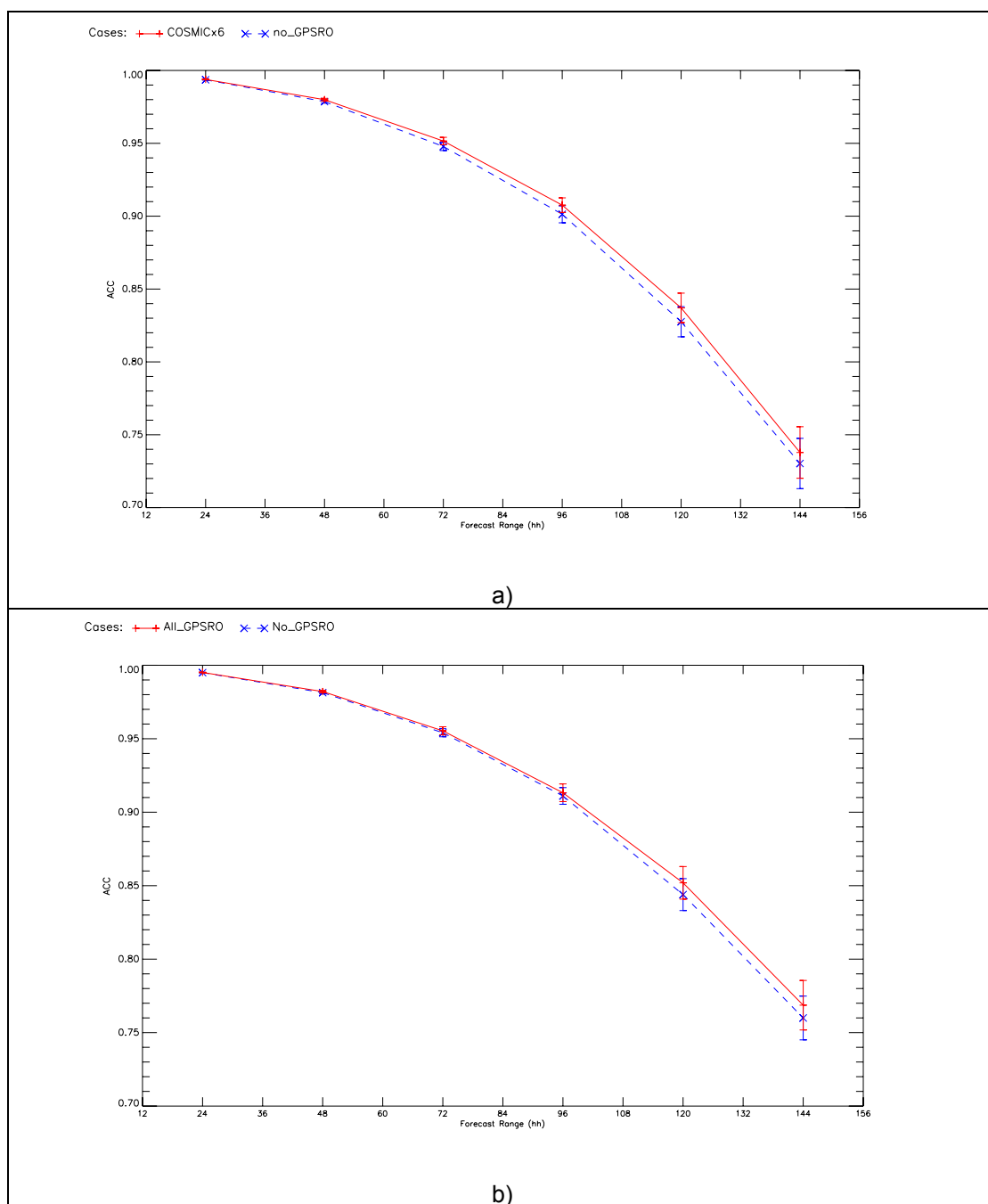
**Figure 27.** COSMICx6 “winter” trial in a) and All\_GPSRO “summer” trial result in b). Mean error (top) and RMS error (bottom) compared to radiosonde temperature (K) at 100 hPa as a function of forecast range in the tropics. The experiments are shown in red and the controls in blue (both with no GPS RO).

Figure 27 shows some fairly small improvements in RMS at 100 hPa temperature in the TR against radiosondes. It is interesting that the “winter” trial has a larger impact on the bias than the “summer”.



**Figure 28.** COSMICx6 “winter” trial in a) and All\_GPSRO “summer” trial result in b). Mean error (top) and RMS error (bottom) compared to radiosonde wind measurements (m/s) at 250 hPa as a function of forecast range in the southern hemisphere. The experiments are shown in red and the controls in blue (both with no GPS RO).

Small improvements in RMS for long forecast range, SH, 250 hPa wind speed can be seen in both “winter” and “summer” in Figure 28.



**Figure 29.** Plot of the 500 hPa geopotential height anomaly correlation for COSMICx6 “winter” trial in a) and All\_GPSRO “summer” trial result in b) in the SH. The experiments are shown in red and the controls in blue (both with no GPS RO).

GPS RO provides a useful increase in the validity of long range forecasts as can be seen by the 500 hPa geopotential height anomaly correlation coefficient scores (which can be regarded as a skill score with reference to climate) in Figure 29. Similar results are obtained for both periods.

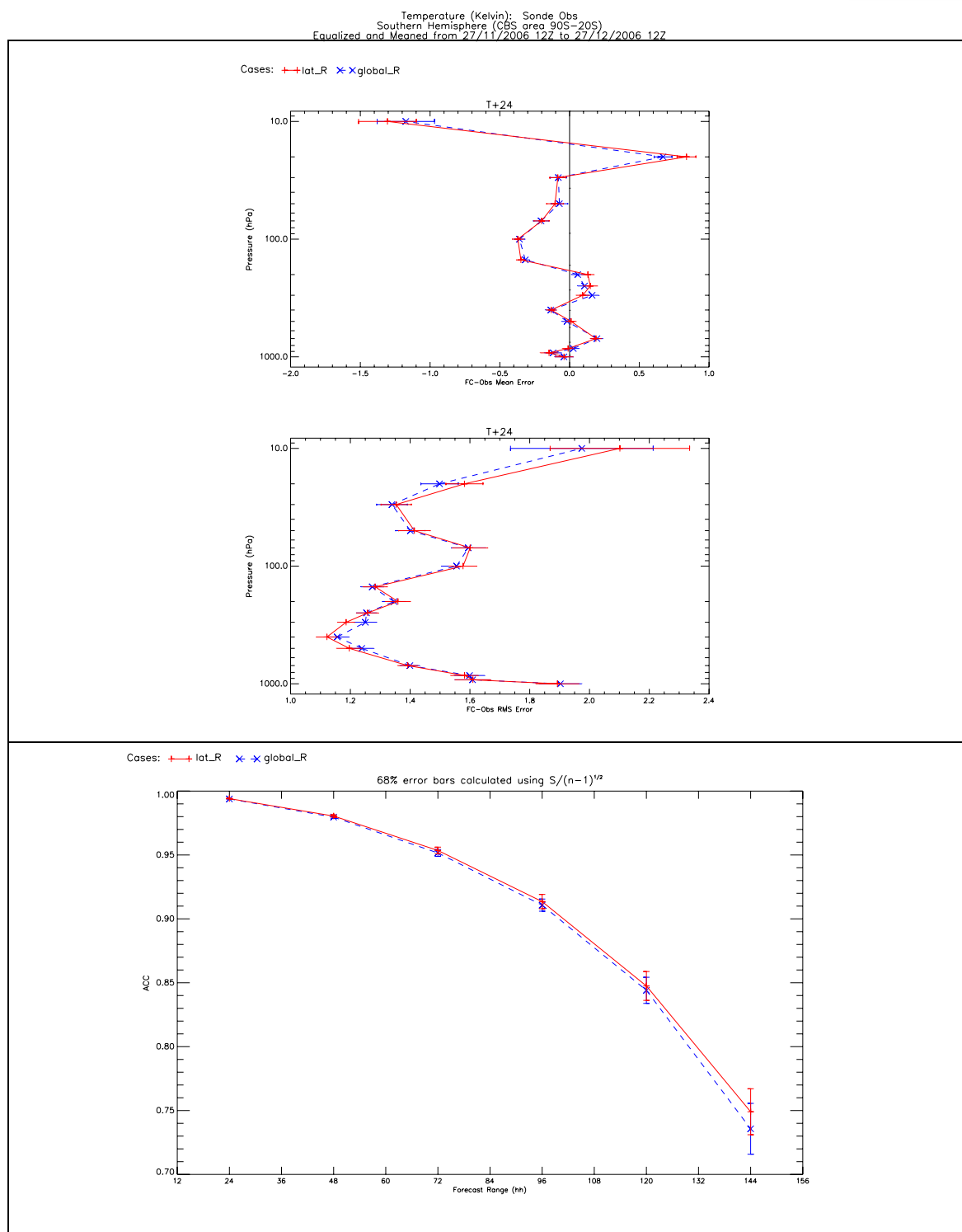


**Figure 30.** latR results in SH. The top image a) shows the mean error and RMS of temperature compared to radiosondes at 24 hour forecast range. The bottom image b) shows the 500 hPa geopotential height anomaly correlation. The experiment is shown in red (with latR setup) and the control in blue (with global **R** matrix).

One can see from Figure 30a that the new **R** matrices in latR show improvement in the range 300, 400, 500 hPa temperatures where the errors are decreased, but a degradation at higher



levels is seen where the errors are increased. Figure 30b shows how the SH 500 hPa geopotential height anomaly correlation coefficient improved using the new latR errors.

## 6. Discussion

It is apparent that GPS RO, in particular COSMIC data, is providing a useful improvement to forecasting skill. For comparison, the recently available data from IASI (onboard MetOp, which provides much greater volumes of data than COSMIC) trialled over the same “summer” period gave  $\sim +1\%$  in NWP index against both observations and analyses, whereas for the same period GPS RO gave (using 0-40 km cut-off)  $\sim +0.9\%$  against observations and  $\sim +0.3\%$  against analysis. Also in the more impressive “winter” period trials GPS RO gave an optimal  $\sim +1.1\%$  in NWP index against observations and  $\sim +0.8\%$  against analyses. Clearly one period is not a great sample for the comparison of the data types, however it still demonstrates that GPS RO is an important data type in an era when it is becoming increasingly difficult to improve forecasts due to the great volumes of data already assimilated. It should be noted that GPS RO and IASI should provide complementary information, see Collard and Healy 2003.

The reasons for poorer performance in “summer” are partly due to a problem with the control (with no GPS RO) not assimilating any data on one 6 hour cycle leading to a poorer analysis NWP index score and also the fact that the availability of GPS RO data was almost reduced to zero on several of the cycles, particularly around late May and late June. Other potential explanations include the meteorological differences between the seasons and that the assimilation system had been improved since the “winter” period.

We believe the issue of whether to assimilate GPS RO refractivity data higher than 27 km has been partly resolved. It is clear that it does not degrade the forecasts (in fact the observation scores are improved a little) and its use in decreasing the upper level ‘S’ shape bias has been demonstrated with a comparison in bending angle space. Refractivity from the GRAS instrument may potentially be used to even higher than 40 km due to better SNR compared to the current available instruments. Both trial periods showed that assimilating with a 0 km lower cut-off provides a small but useful increase in NWP index and with perhaps a bit more refinement regarding the use of variable lower cut-off we should start assimilating lower (it may still be a risk to assimilate to 0 km with a fixed cut-off due to the rare occasions when representativeness error of the 1D forward model is very large).

At the Met Office, radiance measurements are assimilated after a bias correction using the model background. In a model that clearly has some large biases in the stratosphere, as seen in the monitoring comparison to ECMWF, this is far from an ideal scenario for GPS RO assimilation. GPS RO is known to have negligible biases for a good proportion of an occultation profile and thus can be thought of as an “anchor” measurement (similar to radiosondes) for other data that needs to be bias corrected. Therefore until issues regarding bias correction schemes are resolved, radiance measurements may be fighting against GPS RO in some scenarios, which may be limiting GPS RO’s impact.

Although increasing the errors above 10 km led to an improvement in terms of the cost of GPS RO in VAR and a decrease in increment sizes it is clear that this also led to some degradation in the forecast fit to radiosonde temperatures at these altitudes. Given this it appears that our error estimates are still a little large; of course being of the same size as the (O-B)/B standard deviation they are an overestimate. Further tests regarding the **R** matrix values should be done to try and optimise the assimilation.

A next major step in the assimilation of GPS RO would be to assimilate bending angles instead of refractivity. Once we are capable of this, then a detailed experiment to test which

method is best will be undertaken.

## 7. Conclusions

In this paper the implementation of GPS RO data within the Met Office assimilation scheme and results of forecast impact experiments with a focus on COSMIC data have been described. Experiments during two seasons demonstrated a useful improvement in forecast skill as a result of assimilating GPS RO. Hence COSMIC data is now used operationally at the Met Office. The data's most significant impact can be seen in forecast comparisons to radiosonde temperature observations in the southern hemisphere and tropics. In particular at 200 hPa (~11 km) in the southern hemisphere the fit to radiosonde temperatures showed statistically significant improvements in bias at the 0.05 significance level. In the southern hemisphere and tropics other variables showed improvements, but to smaller magnitude than temperature e.g. geopotential height, relative humidity and wind.

The monitoring results showed that the global model has high level biases that are absent in ECMWF's global model. It was also shown that refractivity biases due to differing processing methods (between UCAR and GFZ) still exist above ~27 km, however the magnitude of these processing biases is small enough that the assimilation of refractivity still gives benefit by decreasing high level model biases; this was confirmed in bending angle space. This is a pleasing result as it was thought that processing biases in refractivity may have caused problems.

## Acknowledgements

We acknowledge with thanks Taiwan's National Space Organization (NSPO) and the University Corporation for Atmospheric Research (UCAR) for providing the Data and Data Products from the COSMIC/FORMOSAT-3 mission. The COSMIC/FORMOSAT-3 mission is sponsored by the National Science Council in Taiwan and the National Science Foundation (NSF), National Aeronautics and Space Administration (NASA), National Oceanic and Atmospheric Administration (NOAA), Air Force Office of Scientific Research and Air Force Weather, the Office of Naval Research, and the Space Test Program in the United States. We would also like to thank GFZ for providing CHAMP and GRACE-A data. We would like to thank Dave Offiler (Met Office) for many useful insights into the data, also Sean Healy (ECMWF) for useful discussions on many of the topics in this paper and also for providing ECMWF data for comparison. Steve English (Met Office) also provided useful insight into the verification.

## References

- Ao, C. O., et al, 2003, Lower-troposphere refractivity bias in GPS occultation retrievals, *J. Geophys. Res.*, 108(D18), 4577, doi:10.1029/2002JD003216
- Collard, A. and S. Healy 2003. The combined impact of future space-based atmospheric sounding instruments on numerical weather prediction analysis fields: A simulation study. *Q. J. R. Meteorol. Soc.* 129: 2741–2760.
- Cucurull, L., et al., 2006, Assimilation of Global Positioning Radio Occultation Observations into NCEP's Global Data Assimilation System, *Monthly Weather Review*, Vol:135, p 3174-3193
- Eyre, J., 2004, Assimilation of radio occultation measurements into a numerical weather prediction system, Technical memorandum 199, ECMWF, Reading, UK
- Healy, S. B., 2001, Radio occultation bending angle and impact parameter errors caused by horizontal refractive index gradients in the troposphere: A simulation study. *J. Geophys. Res.*, 106, 11875–11889
- Healy, S. B., et al. (2005a), Forecast impact experiment with GPS radio occultation measurements, *Geophys. Res. Lett.*, 32, L03804, doi:10.1029/2004GL020806
- Healy, S. B. and J.-N. Thépaut (2005b), 4D-Var assimilation experiment with CHAMP GPS radio occultation measurements, *Geophys. Res.*, 7, 031147.
- Healy, S. B. and J.-N. Thépaut (2006), Assimilation experiment with CHAMP GPS radio occultations measurements, *Q. J. R. Meteorol. Soc.*, 132, 605–623.
- Healy, S. B. et al (2007), Assimilating GPS radio occultation measurements with two-dimensional bending angle observation operators, *QUARTERLY JOURNAL OF THE ROYAL METEOROLOGICAL SOCIETY* 133 (626): 1213-1227 Part A
- Kuo, Y. -H. et al.: 2004, Inversion and Error Estimation of GPS Radio Occultation Data, *J. Met. Soc. Japan*, Vol. 82, No. 1B, pp. 507-531
- Kursinski, E., G. Hajj, J. Schofield, R. Linfield and K. Hardy: 1997, Observing earth's atmosphere with radio occultation measurements using the Global Positioning System, *J. Geophys. Res.*, 102, 23429–23465
- Kursinski, E., G. Hajj, S. Leroy and B. Herman: 2000, The GPS Radio Occultation Technique, *TAO*, Vol. 11, No. 1, 53-114
- Melbourne, W. G., et al. (1994), The application of spaceborne GPS to atmospheric limb sounding and global change monitoring, *Jet. Propul. Lab.*, Pasadena, Calif.

Rawlins, F., S. P. Ballard, K. J. Bovis, A. M. Clayton, Dingmin Li, G. W. Inverarity, A. C. Lorenc, T. J. Payne: 2006, The Met Office Global 4D-Var Scheme, *Q. J. Royal Meteor. Soc.*

Schreiner W, Rocken C, Sokolovskiy S, et al., Estimates of the precision of GPS radio occultations from the COSMIC/FORMOSAT-3 mission, *GEOPHYSICAL RESEARCH LETTERS* 34 (4): Art. No. L04808 FEB 23 2007

Steiner, A. K., and G. Kirchengast (2005), Error analysis for GNSS radio occultation data based on ensembles of profiles from end-to-end simulations, *J. Geophys. Res.*, 110, D15307, doi:10.1029/2004JD005251

## Glossary

ATOVS	Advanced TIROS Operational Vertical Sounder
CHAMP	CHAllenging Minisatellite Payload
COSMIC	Constellation Observing System for Meteorology, Ionosphere & Climate
DMI	Danish Meteorological Institute
ECMWF	European Centre for Medium Range Weather Forecasts
GFZ	GeoForschungsZentrum, Potsdam
GPS RO	Global Positioning System Radio Occultation
GRACE-A	Gravity Recovery and Climate Experiment
GRAS SAF	Global Navigation Satellite System Receiver for Atmospheric Sounding Satellite Application Facility
IASI	Infrared Atmospheric Sounding Interferometer
LEO	Low Earth Orbit
MetDB	The Meteorological Database
MetOp	The Meteorological Operational satellite programme
NCEP	National Centers for Environmental Prediction
NH	Northern Hemisphere
NWP	Numerical Weather Prediction
OPS	Observations Processing System
PMSL	Pressure at mean sea level
RMS	Root mean square
ROPP	Radio Occultation Processing Package
SH	Southern Hemisphere
SNR	Signal to noise ratio
TR	Tropics
UCAR	University Corporation for Atmospheric Research
UKMO	UK Met Office
UM	Unified Model
VAR	Variational Data Assimilation System
RTTOV	Radiative Transfer for TOVS